Tellus
SERIES B
CHEMICAL
AND PHYSICAL
METEOROLOGY
PUBLISHED BY THE INTERNATIONAL METEOROLOGICAL INSTITUTE IN STOCKHOLM

Tellus (2010), 62B, 475–496
Printed in Singapore. All rights reserved

TELLUS

Net ecosystem productivity of temperate and boreal forests after clearcutting—a Fluxnet-Canada measurement and modelling synthesis

By R. F. GRANT[1]*, A. G. BARR[2], T. A. BLACK[3], H. A. MARGOLIS[4], J. H. MCCAUGHEY[5] and J. A. TROFYMOW[6], [1]*Department of Renewable Resources, University of Alberta, Edmonton, AB, Canada T6G 2E3;* [2]*Climate Research Branch, Meteorological Service of Canada Saskatoon, SK, Canada S7N 3H5;* [3]*Faculty of Land and Food Systems, University of British Columbia, Vancouver BC, Canada V6T 1Z4;* [4]*Faculté de Foresterie et de Géomatique, Pavillon Abitibi-Price, Université Laval, Québec, PQ, Canada G1K 7P4;* [5]*Department of Geography, Queen's University, Kingston, ON, Canada K7L 3N6;* [6]*Canadian Forest Service, Pacific Forestry Centre, Victoria, BC, Canada V8Z 1M5*

(Manuscript received 28 November 2009; in final form 9 July 2010)

ABSTRACT

Clearcutting strongly affects subsequent forest net ecosystem productivity (NEP). Hypotheses for ecological controls on NEP in the ecosystem model *ecosys* were tested with CO_2 fluxes measured by eddy covariance (EC) in three post-clearcut conifer chronosequences in different ecological zones across Canada. In the model, microbial colonization of postharvest fine and woody debris drove heterotrophic respiration (R_h), and hence decomposition, microbial growth, N mineralization and asymbiotic N_2 fixation. These processes controlled root N uptake, and thereby CO_2 fixation in regrowing vegetation. Interactions among soil and plant processes allowed the model to simulate hourly CO_2 fluxes and annual NEP within the uncertainty of EC measurements from 2003 to 2007 over forest stands from 1 to 80 yr of age in all three chronosequences without site- or species-specific parameterization. The model was then used to study the impacts of increasing harvest removals on subsequent C stocks at one of the chronosequence sites. Model results indicated that increasing harvest removals would hasten recovery of NEP during the first 30 yr after clearcutting, but would reduce ecosystem C stocks by about 15% of the increased removals at the end of an 80-yr harvest cycle.

1. Introduction

Net biome productivity (NBP) of forest ecosystems can be adversely affected by an increased frequency and/or intensity of disturbances such as harvesting, fire and insects. The intensity of harvesting may vary from minimal, as in selective logging where the forest stand remains mostly in place, to severe, as in clearcut logging where the forest stand is completely replaced. Clearcut logging adversely affects NBP through: (1) direct export of C as harvested wood products (2) increased heterotrophic respiration (R_h) driven by decomposition of detritus, including above- and below-ground fine litter and woody debris (WD), left in large amounts after clearcutting and warmed by exposure to solar radiation and (3) slow recovery of net primary productivity (NPP) caused by small leaf areas and root lengths of plants regrowing from seeds or rootstocks under limited nutrient availability. Rates of R_h may exceed those of NPP for several years after clearcutting, during which time substantial losses of ecosystem C stocks may occur. These losses may continue for 10 yr or longer in Canadian forests (Kurz and Apps, 1999; Litvak et al., 2003), for at least 14 yr in Siberian pine forests (Schulze et al., 1999) and for 14 (Janisch and Harmon, 2002) or 20 (Cohen et al., 1996) years in coniferous forests of the Pacific Northwest. Eventually R_h declines as detritus remaining from the previous forest is depleted, while NPP rises as forest leaf area and root length recover, so that the forest starts to regain C.

The time course of C loss and recovery after disturbance strongly affects NBP over the forest life cycle, so that much effort has been invested in measuring and modelling rates of litter decomposition and tree growth after stand-replacing harvests or fires. Approaches to estimating WD losses have differed in complexity. Most researchers (e.g. Janisch and Harmon, 2002; Shorohova et al., 2008; Melin et al., 2009) have derived first-order decomposition rate constants to estimate C losses from

*Corresponding author.
e-mail: robert.grant@ales.ualberta.ca
DOI: 10.1111/j.1600-0889.2010.00500.x

WD stocks following harvest. Shorohova et al. (2008) further proposed different rate constants for bark and wood decomposition while accounting for wood fragmentation. However other researchers (e.g. Mäkinen et al., 2006; Montes and Cañellas, 2006) have found that WD decomposition rates could better be fitted with Gomperz or Chapman–Richards functions in which a time lag was modelled before the onset of substrate-limited decomposition. These functions were based on the observation that decay is slow until heterotrophic decomposers have become established within the substrate (Grier, 1978; Harmon et al., 1986). Montes and Cañellas (2006) further parameterized these functions to allow more rapid decomposition rates in more advanced WD decay classes. Diochon et al. (2009) found that significant post-harvest C losses also occurred in the mineral soil below the forest floor, and so must be included in a full accounting of post-harvest changes in C stocks, although Johnson and Curtis (2001) found no consistent effect of harvesting on soil non-litter C.

Plant regrowth after a stand-replacing disturbance is strongly affected by mineralization of nutrients from forest litter. During the first few years after disturbance, the rapid decomposition of fine plant litter, such as foliar litter with comparatively low C:nutrient ratios can cause a transient net mineralization of nutrients that may stimulate early regrowth of LAI and rise in gross primary productivity (GPP; Kimmins, 2004), mostly by herbaceous pioneer species. However this post-harvest mineralization is sometimes not found, likely when fine litter mineralization is constrained by low pH or nutrient content (Grenon et al., 2009). The concurrent decomposition of large amounts of WD with high C:nutrient ratios immobilizes nutrients (Grier, 1978; Schimel and Firestone, 1989), limiting nutrient uptake by regrowing plants with small root systems, thereby lowering foliar N concentrations (Bradley et al., 2002) and hence GPP (Kimmins, 2004). This constraint on nutrient uptake is gradually relieved as continued decomposition of WD generates products with smaller C:nutrient ratios, allowing eventual remineralization of WD nutrients. This constraint is relieved even further as plant roots proliferate during regrowth, improving their nutrient uptake capacity and allowing LAI and GPP to rise, mostly from dominant tree species. Thus Taylor et al. (2005) developed different Chapman–Richards functions to model the regrowth of trees, seedlings and shrubs after harvest. These functions were parameterized to allow rapid early growth and subsequent decline of seedlings and shrubs, but slow early growth and subsequent faster growth of trees. Similar functions have also been used to simulate early tree growth in inventory-driven models of forest growth (e.g. Kurz et al., 2009).

Most post-harvest models of litter decomposition and forest regrowth have been derived empirically from studies of C inventories in post-harvest chronosequences (summarized in Melin et al., 2009) so that the validity of their parameters is likely to be limited to the conditions of the studies. A more process-based model of decomposition and regrowth might enable a more robust simulation of post-harvest changes in forest C stocks that could be used in life-cycle forest C studies without the need for site-specific parameterization. Such a model should be able to simulate the processes and kinetics of colonization and subsequent decomposition of new detritus stocks, as well as those of older soil organic carbon (SOC) stocks, by heterotrophic decomposers. The model should also be able to simulate the mineralization versus immobilization of N driven by this decomposition, and its effects on plant N uptake during forest regrowth.

Chronosequence studies of post-disturbance changes in C stocks can provide only weak tests of process models because these changes represent temporally aggregated results of disturbance effects on ecosystem processes, rather than effects on the processes themselves. Process-level disturbance effects may be better represented by changes in CO_2 effluxes versus CO_2 influxes measured at eddy covariance (EC) flux towers in post-disturbance chronosequences. These fluxes directly indicate rates of ecosystem respiration versus primary productivity as affected by rates of detritus decomposition versus plant regrowth, and so provide better constrained tests of process models. In this study, we test hypotheses for decomposition and regrowth in the ecosystem process model *ecosys* against EC CO_2 fluxes in three diverse post-clearcut chronosequences in British Columbia (BC), Saskatchewan (SK) and Quebec (QC) as part of the Canadian Carbon Program (CCP). To evaluate model sensitivity to changes in harvest intensity, the model was then used to project long-term effects of different harvest removals on forest C stocks at one site in the BC chronosequence.

2. Model development

2.1. General

The equations and parameters used to model decomposition and growth remain the same as those documented in several earlier modelling studies (e.g. Grant et al., 1993a,b, 2007a,b, 2008, 2009a,b; Grant, 1998, 2004). Those equations particularly relevant to this study are described in more detail below, where key model parameters appear in bold with values given in the Appendix. A fuller description of all algorithms by which decomposition and growth are governed in *ecosys* may be found in 'Appendix A. Supplementary data' available online in Grant et al. (2009a).

2.2. Detritus decomposition

Decomposition of C (D_{SC}) from organic matter (S_C) colonized by microbial C (M_C) occurs concurrently within each of five organic matter–microbe complexes [i = woody debris, fine nonwoody litter, animal manure, particulate organic matter (POC) and humus], each with kinetic components (e.g. j = protein, carbohydrate, cellulose and lignin, where i = woody debris or litter) in each organic substrate (k = original complex matter,

sorbed organic matter or microbial residues) in each soil or litter layer l. Decomposition (D_{SC}) is a temperature-dependent function (f_{tg}) of a specific decomposition rate (D_{SC}) and the active component (a) in the M_C of all heterotrophic functional types (n = obligately aerobic bacteria and fungi, facultatively anaerobic bacteria, anaerobic acetogens, acetotrophic methanogens, aerobic and anaerobic diazotrophs) (first line of eq. 1). D_{SC} is constrained by both substrate and microbial concentrations represented by half-saturation and inhibition constants (K_{mD} and K_{iD}, respectively) (third line of eq. 1):

$$D_{SCi,j,k,l} = D_{SCj} \sum_n M_{Ci,n,a,l} \left\{ S_{Ci,j,k,l} \Big/ \left(\sum_j \sum_k S_{Ci,j,k,l} \right) \right\} \times f_{tgl}\{[S_{Ci,j,k,l}]\} \Big/ \left\{ [S_{Ci,j,k,l}] + K_{mD} \left(1.0 + \left[\sum_n M_{Ci,n,a,l} \right] \Big/ K_{iD} \right) \right\}. \quad (1)$$

The latter constant inhibits D_S as aqueous concentrations of $M_C([M_C] = M_C/\theta)$ rise with declining water content θ during drying of S_C. Decomposition of C drives that of N and P (D_{SN} and D_{SP}):

$$D_{SNi,j,k,l} = D_{SCi,j,k,l}(S_{Ni,j,k,l}/S_{Ci,j,k,l}) \quad (2a)$$

$$D_{SPi,j,k,l} = D_{SCi,j,k,l}(S_{Pi,j,k,l}/S_{Ci,j,k,l}). \quad (2b)$$

2.3. Heterotrophic respiration

Products of D_{SC}, D_{SN} and D_{SP} are added to dissolved pools (Q) of which Q_C is the substrate for temperature-dependent heterotrophic respiration (R_h) according to a specific respiration rate (R_h) constrained by a half-saturation constant (K_{mQ}) (first line of eq. 3)

$$R_{hi,n,l} = R_{hn} M_{Ci,n,a,l}[Q_{Ci,l}]/(K_{mQ} + [Q_{Ci,l}]) \times f_{tgl} \min\{M_{Ni,j,k,l}/(M_{Ci,j,k,l}C_{Nj}),\ M_{Pi,j,k,l}/(M_{Ci,j,k,l}C_{Pj}\} \times (U_{O_2 i,n,l}/U'_{O_2 i,n,l}), \quad (3)$$

where R_h is further constrained by microbial N and P contents (M_N and M_P) with respect to their maximum set concentrations ($\boldsymbol{C}_N$ and $\boldsymbol{C}_P$), and by uptake versus demand for O_2 (U_{O_2} versus U'_{O_2}) (third line of eq. 3) as described in earlier papers cited above. This R_h sustains maintenance and growth respiration (R_m, a temperature-dependent function of M_N, and R_g, respectively)

$$R_{gi,n,l} = \max \left\{ 0,\ R_{hi,n,l} - \sum_j R_{mi,n,j,l} \right\} \quad (4)$$

and R_g drives assimilation of Q_C (U_C) for growth of M_C according to the energy yield (ΔG) versus construction energy cost for microbial growth (E_n), effectively the growth efficiency

$$U_{Ci,n,l} = \min\left(R_{hi,n,l}, \sum_j R_{mi,n,j,l} \right) + R_{gi,n,l}(1 + \Delta G/E_m) \quad (5)$$

with associated assimilation of Q_N and Q_P

$$U_{Ni,n,l} = U_{Ci,n,l}\, Q_{Ni,l}/Q_{Ci,l} \quad (6a)$$

$$U_{Pi,n,l} = U_{Ci,n,l}\, Q_{Pi,l}/Q_{Ci,l}. \quad (6b)$$

Microbial C dynamics are given by the difference between assimilation and respiration R_h (microbial growth) less first-order decay (D_M) allocated to each kinetic component j ($\boldsymbol{F}_j$):

$$\delta M_{Ci,n,j,l}/\delta t = F_j(U_{Ci,n,l} - R_{hi,n,l}) - D_{MCi,n,j,l} \left(R_{hi,n,l} > \sum_j R_{mi,n,j,l} \right) \quad (7a)$$

$$\delta M_{Ci,n,j,l}/\delta t = F_j(U_{Ci,n,l} - R_{mi,n,l}) - D_{MCi,n,j,l} \left(R_{hi,n,l} < \sum_j R_{mi,n,j,l} \right). \quad (7b)$$

2.4. Mineralization and immobilization

The exchange of inorganic N or P between microbial biomass and the soil solution is determined by the ratios between M_C and M_N or M_P resulting from U_C versus U_N or U_P with respect to their maximum set concentrations, for example, for NH_4^+

$$U_{NH_4 i,n,j,l} = M_{C_{i,n,j,l}} C_{Nj} - M_{Ni,j,k,l} \quad (U_{NH_4} < 0 : \text{mineralization}) \quad (8a)$$

$$U_{NH_4 i,n,j,l} = \min\{M_{C_{i,n,j,l}} C_{Nj} - M_{Ni,j,k,l},\ U'_{NH_4} A_{i,n,j,l}([NH^+_{4i,n,j,l}] - [NH^+_{4mn}])/([NH^+_{4i,n,j,l}] - [NH^+_{4mn}] + K_{NH_4})\} \quad (U_{NH_4} > 0 : \text{immobilization}) \quad (8b)$$

and similarly for NO_3^- and PO_4^{2-}. Immobilization is constrained by maximum uptake rate (U'_{NH_4}), microbial surface area (A), minimum concentration ($[NH^+_{4mn}]$) and half-saturation constant (K_{NH_4}). Thus microbial N and P dynamics are given by the difference between uptake U of organic plus inorganic N and P and first-order decay D_M, that accounts for partial recycling of microbial N and P when these are limiting to microbial growth

$$\delta M_{Ni,n,j,l}/\delta t = F_j U_{Ni,nl,} + U_{NH_4 i,n,j,l} + U_{NO_3 i,n,j,l} - D_{MNi,n,j,l} \quad (9a)$$

$$\delta M_{Pi,n,j,l}/\delta t = F_j U_{Pi,nl,} + U_{PO_4 i,n,j,l} - D_{MPi,n,j,l}. \quad (9b)$$

2.5. Colonization of detritus and soil organic matter

S_C added to the organic substrate (k = original complex matter) in each complex (i = woody debris, fine litter, manure, POC or humus) by litterfall or microbial transformation has to be colonized by M_C before decomposition can begin. Other substrates (k = sorbed organic matter, microbial residues) in each complex i are products of microbial transformations and so are considered to be fully colonized. The colonization rate is driven by new microbial growth $U_C - R_h$ in each i from eq. (7a) according to a specific colonization rate β:

$$\delta S_{Ci,j,k,l}/\delta t = \beta \sum_n (U_{Ci,n,l} - R_{hi,n,l})(S'_{Ci,j,k,l}/S'_{Ci,k,l}) \times \{(S'_{Ci,k,l}/S_{Ci,k,l})/(S'_{Ci,k,l}/S_{Ci,k,l} + K_{iS})\}, \quad (10)$$

where S'_C represents the remaining non-colonized k and $S'_{Ci,k,l} = \sum_j S'_{Ci,j,k,l}$. The first S'_C term in brackets allocates colonization of $S\prime_C$ to each kinetic component j, and the second term constrains colonization as S'_C declines with respect to S_C according to an inhibition constant (K_{iS}). This rate then determines $S_{Ci,j,k,l}$ for k = original complex matter in eq. (1).

Colonization of new S'_C (e.g. litterfall) is started by microbial growth from existing S_C in each complex i. S_C grows as colonization proceeds, raising D_{SC} (eq. 1) and hence R_h (eq. 3), R_g (eq. 4), U_C (eq. 5) and $U_C - R_h$, subject to constraints on D_{SC} by litter water content and temperature (eq. 1), and on R_h by microbial temperature and nutrient uptake (eq. 3). These rises drive further growth in S_C (eq. 10), causing a positive feedback cycle in which colonization, decomposition, respiration and microbial growth accelerate. However S_C' declines as colonization proceeds, gradually slowing and eventually reversing this acceleration as opportunity for further colonization diminishes (eq. 10). This algorithm thereby reproduces the dynamics of woody decomposition represented empirically by Gomperz or Chapman–Richards functions in other studies (Mäkinen et al., 2006; Montes and Cañellas, 2006). Values of β and K_{iS} in eq. (10)) were selected to allow large deposits of WD to become fully colonized, corresponding to decay class V as defined by Siitonen et al. (2000), within 10–30 yr of deposition depending on climate, as estimated in WD decomposition models fitted to field measurements by Montes and Cañellas (2006), Müller-Using and Bartsch (2009) and Ranius et al. (2003). However these same values of β and K_{iS} allow more rapid colonization of fine litter in which D_S (eq. 1), R_h (eq. 3), U_C (eq. 5) and hence microbial growth $U_C - R_h$ is faster.

2.6. Gross primary productivity and autotrophic respiration

Canopy GPP (CO_2 fixation) is the sum of that for each leaf surface defined by population, branch, node, layer, azimuth, inclination and exposure (sunlit or shaded), calculated from Farquhar et al. (1980) and coupled to plant water and nutrient status as described in eqs (C1)–(C11) from Grant et al. (2007b) and in eqs (A7f,g,h) in Grant et al. (2010). Products of GPP are added to nonstructural C pools σ_C in branches from where they are transferred to σ_C in roots and from there to mycorrhizae according to concentration gradients of σ_C generated by production versus autotrophic respiration R_a. Below-ground R_a is the sum of that from σ_C (R_c) and that from remobilization of protein structural C (R_s) by population (i = species or cohort) and organ (j = roots or mycorrhizae) in each rooted soil layer l of each order (m = primary or secondary) and node (n)

$$R_a = \sum_i \sum_j \sum_l \sum_m \sum_n (R_{Ci,j,l,m,n} + R_{Si,j,l,m,n}), \quad (11)$$

where R_c is a temperature-dependent function (f_{ta}) of σ_C constrained by uptake (U) versus demand (U') for O_2 and by comparative conductance to nonstructural C transfer g (Grant, 1998)

$$R_{Ci,j,l,m,n} = R'_C \sigma_{Ci,j,l}\, f_{tai,l} \times (U_{O_2 i,j,l}/U'_{O_2 i,j,l}) g_{i,j,l,m,n} \Big/ \sum_m \sum_n g_{i,j,l,m,n} \quad (12)$$

and R_s is driven from maintenance respiration requirements (R_m) unmet by R_c

$$R_{si,j,l,m,n} = -\min\{0,\ R_{ci,j,l,m,n} - R_{mi,j,l,m,n}\}, \quad (13)$$

where R_s drives litterfall l_C of non-protein structural C associated with protein C remobilized by R_s. Growth respiration R_g is the excess of R_c over R_m constrained by root or mycorrhizal turgor (ψ_t) above a threshold value (ψ'_t)

$$R_{gi,j,l,m,n} = \max\{0,\ \min\{(R_{ci,j,l,m,n} - R_{mi,j,l,m,n}) \times \min\{1,\ \max\{0, \psi_{ti,j,l} - \psi'_t\}\}. \quad (14)$$

2.7. Plant growth

R_g drives root and mycorrhizal growth according to their respective growth yields (Y_g) estimated from biochemical composition (e.g. Waring and Running, 1998)

$$\delta M_{Ci,j,l,m,n}/\delta t = R_{gi,j,l,m,n}(1 - Y_{gi,j})/Y_{gi,j} - R_{si,j,l,m,n} - l_{Ci,j,l,m,n} \quad (15)$$

and associated assimilation of N and P according to set ratios for roots. Growth rate ($\delta M_C/\delta t$) drives extension of root and mycorrhizal lengths (L) according to their specific volumes (ν), densities (ρ), internal porosities (θ_P), radii (r) and an assumed cylindrical geometry

$$\delta L_{i,j,l,m,n}/\delta t = \delta M_{Ci,j,l,m,n}/\delta t\, \upsilon_j/\{\rho_j(1 - \theta_{Pi,j})(\pi r_{i,j,l,m^2})\}. \quad (16)$$

Root and mycorrhizal lengths and resulting surface areas (A) determine uptake (U) of inorganic N and P, for example, NH_4^+ in eq. (17), by determining the nutrient concentrations at root and mycorrhizal surfaces ($[NH^+_{4i,j,l}]$) at which radial transport

by mass flow and diffusion, driven by the nutrient concentrations in the soil solution ($[NH_{4l}^+]$) (eq. 17a), equals active uptake by the root and mycorrhizal surfaces, driven by maximum specific uptake (U') and the half-saturation constant (K_{NH_4}) (eq. 17b)

$$U_{NH4i,j,l} = \left\{ U_{wi,j,l}[NH_{4l}^+] + 2\pi \sum_m \sum_n L_{i,j,l,m,n} D_{eNH4l} \times ([NH_{4l}^+] - [NH_{4i,j,l}^+])/\ln(d_{i,j,l}/r_{i,j,l}) \right\} \quad (17a)$$

$$= U'_{NH_4} \sum_m \sum_n A_{i,j,l,m,n}([NH_{4i,j,l}^+] - [NH_{4mn}^+])/[NH_{4i,j,l}^+] - [NH_{4mn}^+] + K_{NH_4}) f_{tsl}. \quad (17b)$$

Parameters for root and mycorrhizal uptake ($U_{NH4i,j,l}$ in eq. 17b) are the same as those for microbial uptake ($U_{NH4i,n,j,l}$ in eq. 8b) with which $U_{NH4i,j,l}$ in eq. (17b) competes. Products of U are added to nonstructural N and P pools (σ_N and σ_P) in root and mycorrhizae which are coupled with σ_C generated from CO_2 fixation, in mycorrhizae, roots and branches. Transfers among these pools (eq. A7a,b in Grant et al., 2010) are driven by concentration gradients generated by acquisition versus consumption of nonstructural N and C in mycorrhizae, roots and branches (eq. A7c,d in Grant et al., 2010). Ratios of nonstructural N and C in branches govern CO_2 fixation (eqs A7f,g,h in Grant et al., 2010) by (1) setting ratios of structural N and C in leaves (eq. A7e in Grant et al., 2010) and hence maximum carboxylation rates (eqs A7i,j in Grant et al., 2010), and (2) determining rubisco activation through product inhibition (eq. A7k in Grant et al., 2010). R_a of above-ground phytomass is calculated from non-structural C pools for each species (i), branch (j), organ (k = leaves, twigs, branches, boles, reproductive) and node (n) in the same manner as is the R_a of roots and mycorrhizae in eqs. (11)–(14) above. Above-ground growth is thus modelled as

$$\delta M_{Ci,j,k,n}/\delta t = F_n R_{gi,j,k}(1 - Y_{gi,k})/Y_{gi,k}] - R_{Si,j,k,n} - l_{Ci,j,k,n} \quad (18)$$

with associated assimilation of N and P, calculated for organ k = leaf from ratios of nonstructural C, N and P as

$$\delta M_{Ni,j,k,n}/\delta t = \delta M_{Ci,j,k,n}/\delta t \; f(\min\{\sigma_{Ni,j}/(\sigma_{Ni,j} + \sigma_{Ci,j}/K_{i\sigma_N}), \sigma_{Pi,j}/(\sigma_{Pi,j} + \sigma_{Ci,j}/K_{i\sigma_P})\}) - l_{Ni,j,k,n} \quad (19a)$$

$$\delta M_{Pi,j,k,n}/\delta t = \delta M_{Ci,j,k,n}/\delta t \; f(\min\{\sigma_{Ni,j}/(\sigma_{Ni,j} + \sigma_{Ci,j}/K_{i\sigma_N}), \sigma_{Pi,j}/(\sigma_{Pi,j} + \sigma_{Ci,j}/K_{i\sigma_P})\}) - l_{Pi,j,k,n} \quad (19b)$$

from which ratios of nonstructural N and C are derived as M_N:M_C.

Growth in leaf mass drives expansion of leaf area (A) constrained by leaf turgor (ψ_t) in eq. (20), assuming uniform growth of individual leaves (M_C divided by population y) in three dimensions (Grant and Hesketh, 1992)

$$\delta A_{i,j,k,n}/\delta t = \alpha(M_{Ci,j,k,n}/y_i)^{-0.33} \times \delta M_{Ci,j,k,n}/\delta t \; \min\{1, \max\{0, \psi_{ti} - \psi'_t\}. \quad (20)$$

Similarly, growth in twig, branch and bole masses drive extension of twig, branch and bole lengths (Grant and Hesketh, 1992). Values of $A_{i,j,k,n,}$ further resolved into layer, azimuth and inclination, are used to calculate radiation absorption and hence CO_2 fixation coupled to leaf water and nutrient status (Grant, 2004; Grant et al., 2007a,b, 2009a,b, 2010).

Each plant population is initialized only with a small nonstructural C reserve at planting which is transferred to σ_C in branches and roots during germination. These σ_C then drive initial R_a (eq. 12) and $\delta M_C/\delta t$ (eq. 15) and hence root elongation (eq. 16) and leaf expansion (eq. 20) required for nutrient uptake (eq. 17) and CO_2 fixation. Upon exhaustion of this reserve, each population must sustain further nutrient uptake and CO_2 fixation from root elongation and leaf expansion driven by the non-structural products of nutrient uptake and CO_2 fixation. No areas or lengths of roots, mycorrhizae or leaves are prescribed. This creates feedback during plant growth, which can be positive when growth exceeds litterfall, or negative when growth does not.

3. Model experiment

3.1. Model initialization and spinup

The different sites at which EC flux towers were maintained in the three post-clearcut chronosequences (BC-HDF, SK-HJP and QC-HBS) are described in Table 1 and in references cited therein. EC measurement methodology followed standard CCP protocol at each site, as described in these references and online at http://www.fluxnet-canada.ca/home.php?page=home&setLang=en. All towers had a fetch longer than 1 km, with footprints within the fetch except under very stable nighttime conditions when measurements were rejected. Before evaluating model performance against CO_2 fluxes measured at these sites, the model had first to reproduce site conditions by simulating site histories. This was accomplished by initializing *ecosys* at each site with the biological properties of the key tree and understory species, represented as plant functional types, and with the physical and chemical properties of the dominant soil type at each site (Table 1). Each plant functional type (coniferous or deciduous, tree or understory) had identical properties at each site in which it was present, except for those properties

Table 1. Key attributes of vegetation, soils and climates at CCP post-clearcut chronosequences and reference forest sites

Site	BC-HDF00	BC-HDF88	BC-DF49	SK-HJP02	SK-HJP94	SK-HJP75	SK-SOJP	QC-HBS00	QC-EOBS
Latitude N	49.9	49.5	49.9	53.9	53.9	53.9	53.9	49.3	49.7
Longitude W	125.3	124.9	125.3	104.7	104.7	104.7	104.7	74.0	74.3
Altitude (m)	175		300	580	580	534	580		
MAT (°C)	8.8	9.6	8.3	1.3	1.4	1.2	0.4	0.0	0.0
Precip. (mm yr^{-1})	1410	1610	1461	417	413	414	467	961	961
Stand Establishment	Clearcut, pile burn planted 2000	Clearcut, slash fire, planted 1988	Fire and clearcut 1938 &43[c], plant 1949	Clearcut 2002 natural regeneration	Clearcut 1994 natural regeneration	Clearcut 1975 natural regeneration	Wildfire 1916	Whole tree clearcut 2000, planted 2004	Fire 1898
Area (ha)	32	110	130	49	26	73	494	109	>400
Height (m)	2.4 (2008)	7.5 (2008)	33 (2008)	0 (2002)	1.7 (2002)	7.6 (2002)	16.7 (2002)	0.25 (2005)	13.8 (2004)
Density (ha^{-1})	1500	1240	1100	0	12500	7000	1900	2000	4490
Dominant Overstory	Douglas fir	Douglas fir	Douglas fir	Jack pine	Jack pine	Jack pine	Jack pine	Black spruce	Black spruce
Other Overstory	Western red cedar	Western red cedar	Western red cedar, western hemlock	None	None	None	None	Jack pine	Jack pine
Understory	Dense fern, fireweed, salal, bearberry	Dense salal, fern, currant, willow	sparse salal, fern, moss	Bearberry, green alder, feathermoss	Bearberry, green alder, feathermoss	Lichen, green alder	Lichen, green alder	Blueberry, laurel, feathermoss	Feathermoss, sphagnum
Soil Type	Humo-ferric podzol	Humo-ferric podzol	Humo-ferric podzol	Brunisol	Brunisol	Brunisol	Glzacial till	Ferro-humic podzol, organic	Ferro-humic podzol
LFH (cm)	3.6 ± 4.8	4.1 ± 3.3	3.0 ± 2.1	0.2	0.3	3	5	40	27
LFH C:N	87	60	48	69	31	44	52	52	52
Mineral soil texture	Gravelly sandy loam	Gravelly loam	Gravelly sandy loam	Sand	Sand	Sand	Sand	Gravelly loamy sand	Gravelly loamy sand
Mineral soil C:N (0–10 cm)	29	29	34	36	40	32	22	29	29
Harvest Removal[a]	0,0,0.7,0	0,0,0.4,0[b]	0,0,0.8,0.8[c]	0,0,0.6,0	0,0.0.6,0	0.6,0.6,0.8,0	n/a	0.1,0.1,0.4,0	n/a
Period of measurement	2001–2007	2002—2007	1998–2007	2003–2007	2002–2005	2004–2007	2000–2006	2002 – 2007	2004–2007
Recent site references	Jassal et al. (2007, 2009); Schwalm et al. (2007); Humphreys et al. (2005), Trofymow et al. (2008).			Howard et al. (2004); Mkhabela et al. (2009); Zha et al. (2009)				Bergeron et al. (2008); Giasson et al. (2006)	
Ecosys references	Grant et al. (2007b, 2009a)			Grant et al. (2007a, 2009a)				Grant et al., (2008, 2009a)	

[a]Fractional removal of foliage, other non-woody phytomass, living wood and standing dead wood, respectively, used to simulate clearcutting,

[b]Followed by slash burn in 1988,

[c]1938 part clearcut, 1939 slash fires and burns into some remaining timber, 1943 salvage logging and clearcut, 1943 slash burn.

associated with timing of key phenological events such as leaf flush and reproductive growth (e.g. Grant et al., 2007a) which were adapted to the climate zone (temperate or boreal) at each site. All plant properties were derived from independent experiments and so remained unchanged from those used in earlier studies (e.g. Grant et al., 2007b, 2008, 2009a).

Ecosys was also initialized with stocks of WD and fine litter estimated to remain after a stand-replacing fire in a model year corresponding to the late 18th or early 19th century, depending on site history. The model was then run from forest seeding to maturity (ca. 100 yr) under repeating sequences of continuous hourly weather data (radiation, air temperature, dewpoint or RH, wind speed and precipitation) recorded during the period of measurement at each site (Table 1). The modelled forests were then clearcut or burned, depending on site history, in the model year corresponding to that in which the most mature forest stands (BC-DF49, SK-SOJP and QC-EOBS) were disturbed (Table 1). These disturbances used removal coefficients for foliage, other non-woody phytomass, living and standing dead wood derived from Kurz et al. (2009). All remaining phytomass was transferred to standing dead stocks, or to WD and fine non-woody litter stocks on the ground surface and in the soil profile (dead fine and woody roots). Standing dead stocks were transferred to surface WD stocks using a first-order hourly rate constant that gave a mean residence time in standing dead stocks of about 10 yr. Overstory and understory species were then reseeded and regrown under continuing sequences of weather data until they reached the age of the mature forest sites during the period of EC measurements.

To simulate the recently clearcut sites (BC-HDF00, BC-HDF88, SK-HJP02, SK-HJP94, SK-HJP75 and QC-HBS00), alternative runs were started at the beginning of the model year corresponding to that of the clearcut at each site (Table 1), using values for all state and driver variables stored at the end of the previous year from the model runs for the mature forest sites. The stands were then clearcut on harvesting dates reported from each site using removal coefficients for foliage, other non-woody phytomass, living and standing dead wood derived from Kurz et al. (2009) or from local observations (e.g. Grant et al., 2007b) (Table 1). The stands were then reseeded with tree and understory species on planting dates reported from each site, and regrown under continuing sequences of hourly weather data until they reached the age of the clearcut forest stands during the period of EC measurements.

The model was thus run at all sites for ca. 200 yr before comparison with measured data, so that model results were independent of initial conditions. A background mortality rate of 1.2% (QC-EOBS) or 0.8% (all other sites) per year was applied to forest stands during the model runs, simulating natural self-thinning (Aakala et al., 2007). These rates were applied monthly to populations with trees of uniform biomass, so that both biomass and population were reduced to the same extent by each mortality event. All biomass removed by mortality was added to surface or subsurface detritus stocks in the model. During the last 150 yr of the model runs, atmospheric CO_2 concentration (C_a) rose exponentially from 280 to 385 μmol mol^{-1}, and precipitation NH_4^+ and NO_3^- concentrations used to simulate wet N deposition rose exponentially from historical values based on Holland et al. (1999) to current values based on Meteorological Service of Canada (2004). Atmospheric concentration of NH_3 used to simulate dry N deposition was maintained at 0.0025 μmol mol^{-1}.

3.2. Model testing

Yearly regressions were conducted of modelled hourly CO_2 fluxes on EC hourly averaged CO_2 fluxes at each site in the three chronosequences for all years of measurement from 1 January 2001 to 31 December 2007. Model performance was evaluated from regression intercepts ($a \rightarrow 0$), slopes ($b \rightarrow 1$) and correlation coefficients ($R^2 \rightarrow 1$), and from comparisons of root mean squares for differences between EC and modelled fluxes (RMSD) with root mean squares for error in EC fluxes (RMSE). Values of RMSE at each site-year were calculated as the pooled root mean square of uncertainty in 1/2-hourly EC fluxes during the year using equations for CO_2 random flux measurement errors derived over comparable forest stands by Richardson et al. (2006). Values of NEP from *ecosys* were then compared with those derived from EC fluxes at hourly, daily and annual time scales, gap-filled according to established FCRN protocol described in Barr et al. (2004).

Comparisons were also made of modelled and measured C stocks in live aboveground tree biomass (bole, branches and foliage), live understory, and down WD (coarse, medium and small size classes >1 cm, but excluding stumps, standing dead, fine WD <1cm and surface LFH layers) in groundplots located in each site, which had been measured following guidelines established for Canada's National Forest Inventory (NFI Taskforce 2008). The simple average of multiple groundplots within each site was calculated for comparison and therefore may not reflect the spatial variation in C stocks within the tower footprint and true site mean as noted by Chen et al. (2009). Modelled near-surface soil temperatures were also compared with values measured at differently aged sites.

3.3. Model projections

Model sensitivity to changes in harvesting practices on ecosystem C stocks during subsequent forest regrowth was examined by running *ecosys* at BC-HDF88 for 80 yr after clearcutting in 1988 under repeating sequences of 1988–2007 weather data. Runs were conducted with removal coefficients for foliage, other non-woody phytomass, and living wood used in the model tests (Table 1), and then raised by 0.2 and 0.4 to simulate the effects on NEP of greater bole wood and aboveground detritus removal as might occur with whole tree and bioenergy harvests.

4. Results

4.1. Tests of modelled versus measured CO_2 fluxes

Regression parameters of hourly CO_2 fluxes modelled versus measured during the entire year were poor ($b < 0.8$, $R^2 < 0.5$) for the recent clearcut sites during most years (BC-HDF00, SK-HJP02, SK-HJP94 and QC-HBS00 in Table 2). These parameters improved somewhat ($1.0 > b > 0.8$, $R^2 > 0.6$) in the 10–20-year-old post-clearcut sites (BC-HDF88 and SK-HJP75), and further ($1.2 > b > 1.0$, $R^2 > 0.75$) in the older forest sites (BC-DF49, QC-EOBS). For all site-years, RMSD between modelled and measured hourly CO_2 fluxes was similar to or smaller than RMSE of EC fluxes calculated with the algorithm of Richardson et al. (2006) (Table 2). This indicated that much of the variance in EC fluxes not explained by the model could be attributed to random errors in flux measurements. Therefore better agreement between modelled and measured fluxes than that shown in Table 2 could not conclusively be attributed to improved model performance.

The poorer model performance in the more recently clearcut sites was attributed to low diurnal variation in EC CO_2 fluxes. Consequently variation in EC fluxes associated with surface boundary conditions and therefore amenable to modelling remained small relative to EC random error. Diurnal variation in EC fluxes was greater with respect to random error in the older forest sites (SK-HJP75, QC-EOBS and particularly BC-DF49), so that the model was able to explain a larger fraction of variation in the measured fluxes (Table 2).

4.2. Changes in hourly and daily CO_2 exchange with time after clearcutting

Both influxes and effluxes of hourly CO_2 measured and modelled during the period of most rapid CO_2 exchange in late June increased with time since clearcutting in the BC-HDF (Fig. 1), SK-HJP (Fig. 2) and QC-HBS (Fig. 3) chronosequences. In each of the recently clearcut sites (BC-HDF00 in Fig. 1, SK-HJP02 in Fig. 2 and QC-HBS in Fig. 3), CO_2 effluxes measured and modelled during the first 5 yr after clearcutting were driven by R_h which increased gradually with colonization (eq. 10) and consequent accelerated decomposition (eq. 1) of the substantial amounts of WD and fine litter left from clearcutting. Decomposition at these sites was hastened by higher soil temperatures (Fig. 4) that arose in the model from solving the surface energy balance under increased exposure to incoming radiation caused by low tree and understory LAI. CO_2 effluxes were larger in the 10–20-year-old post-clearcut sites (BC-HDF88 in Fig. 1, SK-HJP94 in Fig. 2) and rose little further in the older forest sites (BC-DF49 in Fig. 1, SK-HJP75 in Fig. 2, QC-EOBS in Fig. 3), as declines in R_h modelled from declining detritus stocks (eq. 10) and temperatures (Fig. 4) offset rises in R_a modelled with tree growth (eq. 11).

CO_2 influxes rose gradually after clearcutting and reseeding from near zero values in the recently clearcut boreal sites (SK-HJP02 in Fig. 2 and QC-HBS in Fig. 3), through intermediate values in the 10–20-year-old post-clearcut sites (BC-HDF88 in Fig. 1, SK-HJP94 in Fig. 2), to maximum values in the older forest sites (BC-DF49 in Fig. 1, SK-HJP75 in Fig. 2 and QC-EOBS in Fig. 3). Influxes modelled during the first decade after clearcutting were mostly from pioneer deciduous plant functional types, much of which contributed to CO_2 effluxes through litterfall, while those modelled thereafter were mostly from dominant tree functional types (Table 1). In the model, these influxes rose because forest regrowth drove root elongation (eq. 16) and leaf expansion (eq. 20) that gradually raised nutrient uptake (eq. 17) and CO_2 fixation (eqs C1 to C11 from Grant et al., 2007b) through further elongation and expansion. Larger CO_2 influxes raised σ_C and hence R_a, thereby raising the autotrophic contribution to CO_2 effluxes. Influxes eventually stabilized in older forest stands as further root elongation and leaf expansion gave declining increments in nutrient uptake and CO_2 fixation but rising increments in senescence and litterfall (eqs 13, 15 and 18). Consequently declines in R_h and rises in R_a eventually ended with rising litterfall, mortality, and slowing growth, causing R_e to stabilize in the older forest stands.

Modelled rises in CO_2 influxes were constrained in all three chronosequences by low leaf N concentrations (eqs A7e-k in Grant et al., 2010), calculated in the model as $(M_N + \sigma_N)/(M_C + \sigma_C)$ (eq. 19) (Table 3). These concentrations were smaller than 0.029 g N g C^{-1} below which growth of Douglas fir was found to be N-limited by Hopmans and Chappell (1994). The early rise and subsequent decline in leaf N concentrations modelled with time since clearcut in the BC chronosequence was consistent with that measured in Douglas-fir clearcuts by Bradley et al. (2002) and in Mountain hemlock by Titus et al. (2006). However the decline measured in the SK chronosequence was smaller than that modelled, possibly because of variation in soil quality among the chronosequence sites (table 1 in Mkhabela et al., 2009).

These low leaf N concentrations were caused in the model by competition for nutrient uptake with heterotrophic microbial populations colonizing WD and soil litter layers (eq. 10) with large C:N and C:P ratios. These ratios (Table 1) were larger than 28:1, above which growth of Douglas fir was found to become N-limited by Edmonds and Hsiang (1987). These ratios slowed decomposition and assimilation of N and P with respect to C (eqs. 2 and 6), forcing immobilization of mineral N and P (eq. 8b) and thereby slowing root and mycorrhizal uptake (eq. 17) and transfer to leaves (eq. A7b in Grant et al., 2010).

In spite of N limitations, CO_2 influxes rose more with time since clearcutting than did CO_2 effluxes at all three chronosequences (Figs 1–3), causing daily modelled and EC-derived NEP to increase (Figs 5–7). This increase was particularly apparent after N fertilization in early 2007 at BC-HDF88 and BC-DF49 (Grant et al., 2010), although not in EC-derived NEP at

Table 2. Intercepts (a), slopes (b), coefficients of determination (R^2), root mean square of differences between modelled and measured fluxes (RMSD), root mean square of error in measured fluxes (RMSE) calculated from Richardson et al. (2006), and number of accepted eddy covariance (EC) fluxes (n) from regressions of hourly modelled CO_2 fluxes versus hourly-averaged EC CO_2 fluxes from 2001 to 2007 at sites regenerating after clearcutting in 2002 (SK-HJP02), 2000 (BC-HDF00,QC-HBS00), 1994 (SK-HJP94), 1988 (BC-HDF88), 1975 (SK-HJP75) and at nearby mature sites (BC-DF49, SK-SOJP, QC-EOBS)

Site	Year	a (μmol m^{-2} s^{-1})	b	R^2	RSMD (μmol m^{-2} s^{-1})	RMSE (μmol m^{-2} s^{-1})	n
BC-HDF00	2001	−0.2	0.50	0.14	1.4	1.9	2877
	2002	−0.2	0.86	0.40	1.4	1.8	3797
	2003	−0.2	1.06	0.40	1.5	1.8	3867
	2004	−0.1	1.07	0.49	1.8	2.0	4190
	2005	−1.2	0.90	0.56	2.3	2.1	4158
	2006	−0.3	1.25	0.58	1.8	1.8	4204
	2007	−0.1	1.21	0.64	2.0	2.1	4145
BC-HDF88	2002	0.0	0.94	0.68	2.6	2.6	3937
	2003	0.5	0.94	0.54	2.8	2.5	3717
	2004	0.5	0.98	0.69	2.8	2.7	5009
	2005	0.4	0.83	0.75	3.0	2.9	4934
	2006	0.5	0.89	0.68	2.9	2.7	4630
	2007	0.9	0.93	0.80	3.0	3.2	4860
BC-DF49	2001	0.4	1.01	0.77	3.3	3.5	4990
	2002	0.5	1.07	0.75	3.4	3.5	5026
	2003	0.3	1.04	0.77	3.4	3.6	5277
	2004	0.6	0.99	0.75	3.8	4.0	4362
	2005	0.9	0.96	0.77	3.8	4.0	4388
	2006	0.1	1.02	0.76	3.4	3.6	5233
	2007	0.4	1.04	0.80	3.4	3.7	5235
SK-HJP02	2003	−0.5	0.29	0.13	0.7	1.2	4009
	2004	−0.2	0.42	0.22	0.6	1.2	5451
	2005	−0.3	0.54	0.21	0.6	1.4	5673
	2006	−0.2	0.53	0.24	0.8	2.1	6300
	2007	0.0	0.63	0.29	0.9	2.3	5619
SK-HJP94	2002	0.2	1.00	0.46	1.0	1.4	4751
	2003	−0.1	0.99	0.42	0.9	1.5	5506
	2004	0.1	0.68	0.45	1.4	1.6	5708
	2005	0.1	0.77	0.55	1.4	1.7	4429
SK-HJP75	2004	0.3	1.01	0.65	1.8	1.9	3654
	2005	0.3	1.05	0.64	1.7	1.7	5630
	2006	0.3	1.19	0.65	1.6	1.7	4537
	2007	0.3	1.03	0.62	1.9	1.9	4849
SK-SOJP	2001	0.5	1.12	0.63	1.6	1.8	5295
	2002	0.3	1.12	0.63	1.5	1.7	5188
	2003	0.2	1.02	0.57	1.6	1.8	5380
	2004	0.2	1.12	0.69	1.4	1.7	4762
	2005	0.2	1.07	0.66	1.5	1.8	5633
	2006	0.2	1.14	0.69	1.3	1.7	4801
	2007	0.2	1.13	0.68	1.6	1.8	5384
QC-HBS00	2002	−0.1	0.96	0.63	0.8	1.4	3684
	2003	−0.1	0.64	0.44	1.1	1.5	4978
	2004	0.2	0.67	0.44	1.1	1.5	4392
	2005	−0.1	0.84	0.60	1.0	1.5	5302
	2006	0.0	0.84	0.64	1.0	1.5	5141
	2007	−0.1	0.55	0.38	1.4	1.5	5453

Table 2. Continued

Site	Year	a (μmol m^{-2} s^{-1})	b	R^2	RSMD (μmol m^{-2} s^{-1})	RMSE (μmol m^{-2} s^{-1})	n
QC-EOBS	2004	0.0	0.90	0.74	1.6	2.0	5305
	2005	0.2	1.00	0.77	1.5	1.9	6522
	2006	0.1	1.03	0.78	1.4	1.9	6362
	2007	0.2	1.09	0.73	1.4	1.8	6391

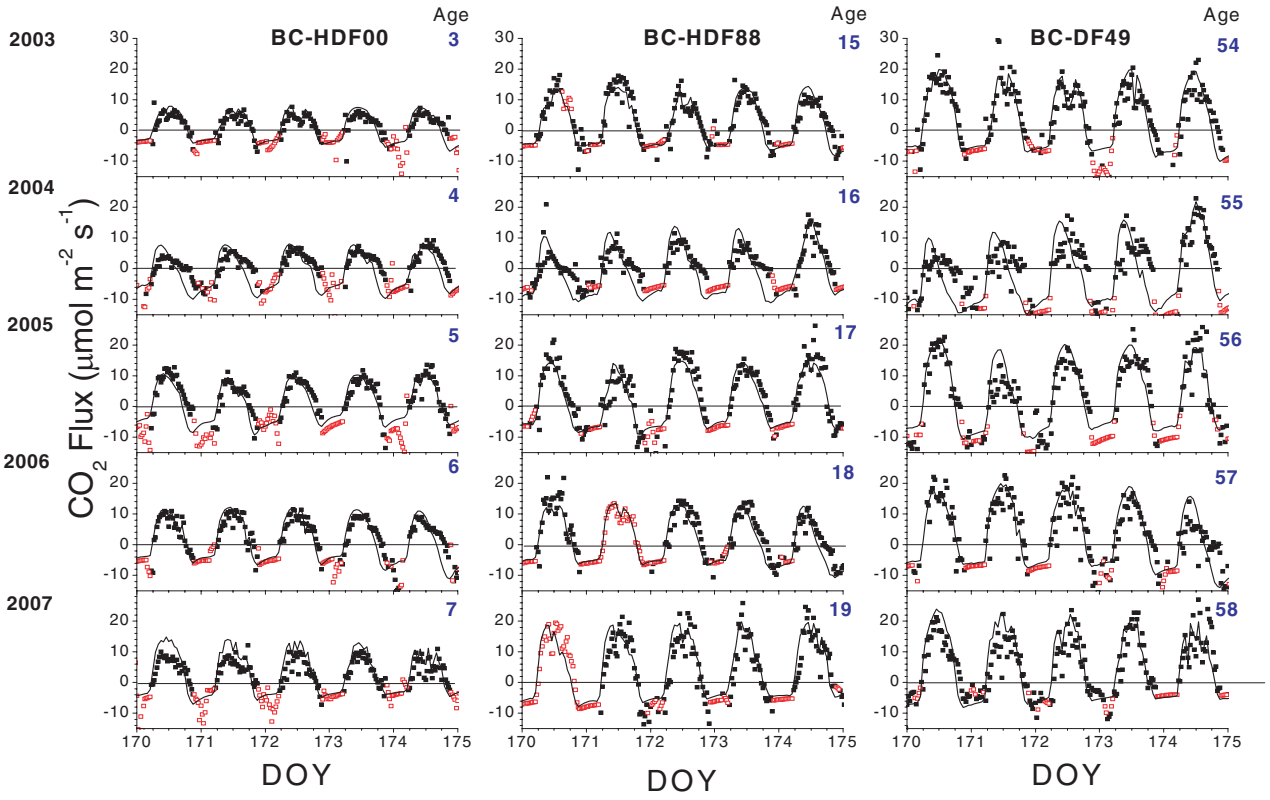

Fig. 1. Hourly CO_2 fluxes measured (closed symbols), gap-filled (open symbols) and modelled (lines) at BC-HDF00, BC-HDF88 and BC-DF49 during DOY 171–175 from 2003 to 2007. Positive or negative values denote CO_2 influxes or effluxes, respectively. BC-HDF00, BC-HDF88 and BC-DF49 stands were fertilized with 6, 20 and 20 g N m^{-2}, respectively, as urea in early 2007.

BC-HDF00 (Fig. 5). CO_2 influxes measured and modelled in recently clearcut sites generally failed to offset CO_2 effluxes (BC-HDF00 in Fig. 1, SK-HJP02 in Fig. 2 and QC-HBS00 in Fig. 3), causing these sites to be net sources of C during 2003–2007 (BC-HDF00 in Fig. 5, SK-HJP02 in Fig. 6 and QC-HBS00 in Fig. 7). CO_2 influxes measured and modelled in the 10–20-year-old post-clearcut sites more fully offset CO_2 effluxes at the two sites for which measurements were available (BC-HDF88 in Fig. 1, SK-HJP94 in Fig. 2), causing these sites to be nearly C neutral during this period (BC-HDF88 in Fig. 5, SK-HJP94 in Fig. 6). CO_2 influxes measured and modelled in the older forests were greater than CO_2 effluxes (BC-DF49 in Fig. 1, SK-HJP75 in Fig. 2 and QC-EOBS in Fig. 3), so that all older sites were net C sinks (BC-DF49 in Fig. 5, SK-HJP75 in Fig. 6 and QC-EOBS in Fig. 7). The seasonal pattern of modelled NEP also changed with time since clearcutting as the early pioneer vegetation dominated by deciduous functional types (BC-HDF00 in Fig. 5, SK-HJP02 and SK-HJP94 in Fig. 6 and QC-HBS00 in Fig. 7) were succeeded by sapling and then closed forests dominated by tree functional types (BC-HDF88 and BC-DF49 in Fig. 5, SK-HJP75 in Fig. 6 and QC-EOBS in Fig. 7).

CO_2 fluxes modelled and measured during forest regrowth were also affected by weather. For example at the BC sites, influxes rose and effluxes declined with cooling during DOY 171–175 in 2004 while influxes declined and effluxes rose with warming during the same DOY in 2006 (Fig. 1).

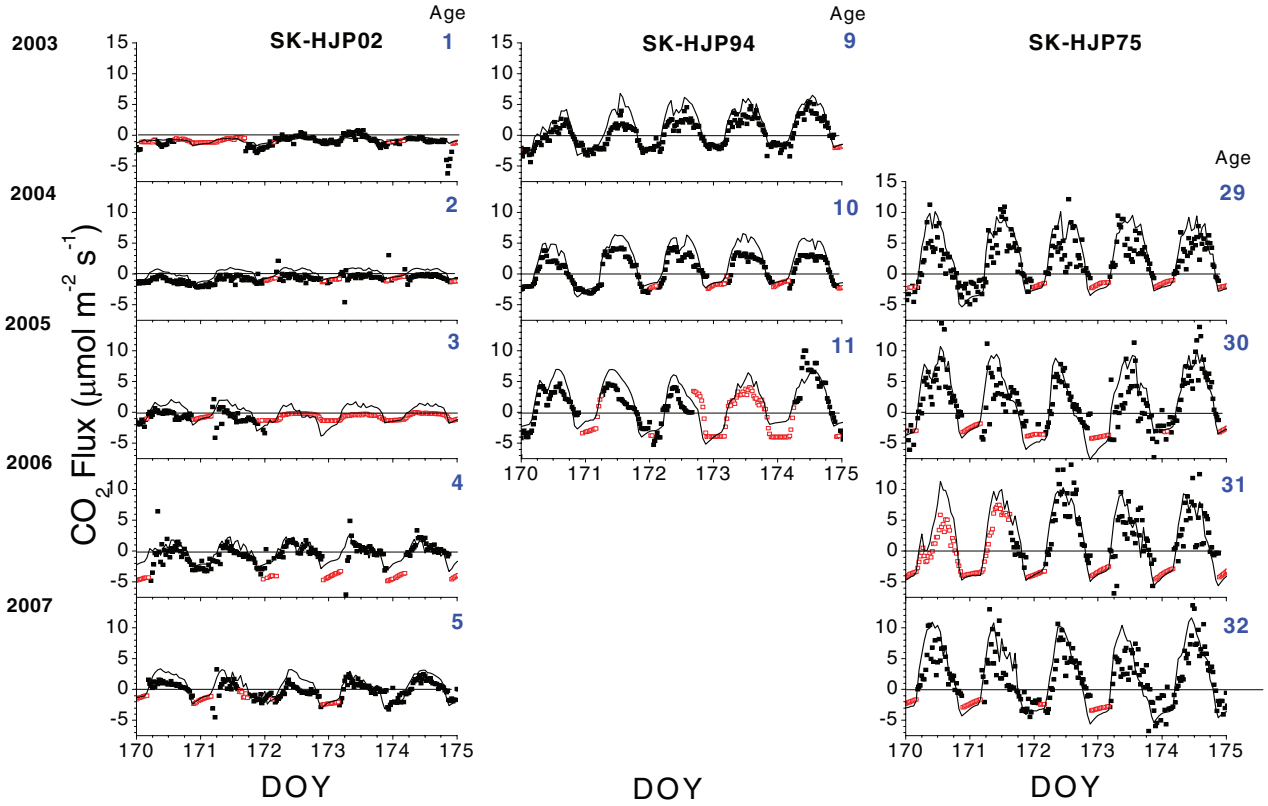

Fig. 2. Hourly CO_2 fluxes measured (closed symbols), gap-filled (open symbols) and modelled (lines) at SK-HJP02, SK-HJP94 and SK-HJP75 during DOY 171–175 from 2003 to 2007. Positive or negative values denote CO_2 influxes or effluxes, respectively.

Consequently NEP at the BC sites was adversely affected by periods of warm weather, notably during the very warm summer of 2004 (Fig. 5). These effects of weather were greater in the older forest site (DF49) due to greater phytomass and greater hydraulic constraints in taller trees as described in Grant et al. (2007b).

4.3. *Changes in annual respiration and productivity with time after clearcutting*

Colonization (eq. 10) and decomposition (eq. 1) of WD and fine litter caused annual rates of modelled R_h and R_e to rise gradually for the first 5 yr after clearcutting (BC-HDF00, SK-HJP02 and QC-HBS00 in Table 4), to maintain larger values during the second decade after clearcutting (BC-HDF88 and SK-HJP94 in Table 4), and to rise little thereafter (BC-DF49, SK-HJP75, SK-SOJP and QC-EOBS in Table 4), consistent with EC-derived R_h (Table 4) and CO_2 effluxes (Figs 1–3). In the model, the small rises in R_e from the older stands were attributed to rises in R_a, offset in some cases by declines in R_h (e.g. BC-DF49 in Table 4).

WD decomposition rates modelled at BC-HDF88 and SK-HJP94 remained low for several years after clearcutting while WD colonization was starting, but rose gradually to 0.05 and 0.025 yr^{-1}, respectively after about 10 yr as colonization progressed (Fig. 8), comparable to rates for wood derived in similar ecozones from litterbags (Trofymow et al., 2002) and for WD in other chronosequence studies (Næsset, 1999; Janisch and Harmon, 2002; Shorohova et al., 2008; Melin et al., 2009). These rates allowed WD modelled at BC-HDF88 to approach full colonization after 20 yr (colonized WD approaching total remaining WD in Fig. 8), consistent with the time course of WD decomposition stages estimated in Ranius et al. (2003). Most WD at BC-HDF88 was observed to have reached decomposition class 3 in 2002 (Trofymow, FCRN DIS at http://fluxnet.ccrp.ec.gc.ca), consistent with the partial colonization modelled at this site in 2002 (Fig. 8).

Modelled and EC-derived GPP were much smaller than R_e in recently clearcut sites (BC-HDF00, SK-HJP02 and QC-HBS00 in Table 4), but rose more rapidly with time, approaching R_e in the 10–20-year-old post-clearcut sites (BC-HDF88 and SK-HJP94 in Table 4), and surpassing R_e in the older forest stands 30–105 yr after disturbance (BC-DF49, SK-HJP75, SK-SOJP and QC-EOBS in Table 4). The greater rise in GPP versus R_e with time since clearcutting arose from the greater rises in CO_2 influxes versus effluxes (Figs 1–3), causing rises in daily NEP (Figs. 5–7) that caused those in annual NEP (Table 4). These

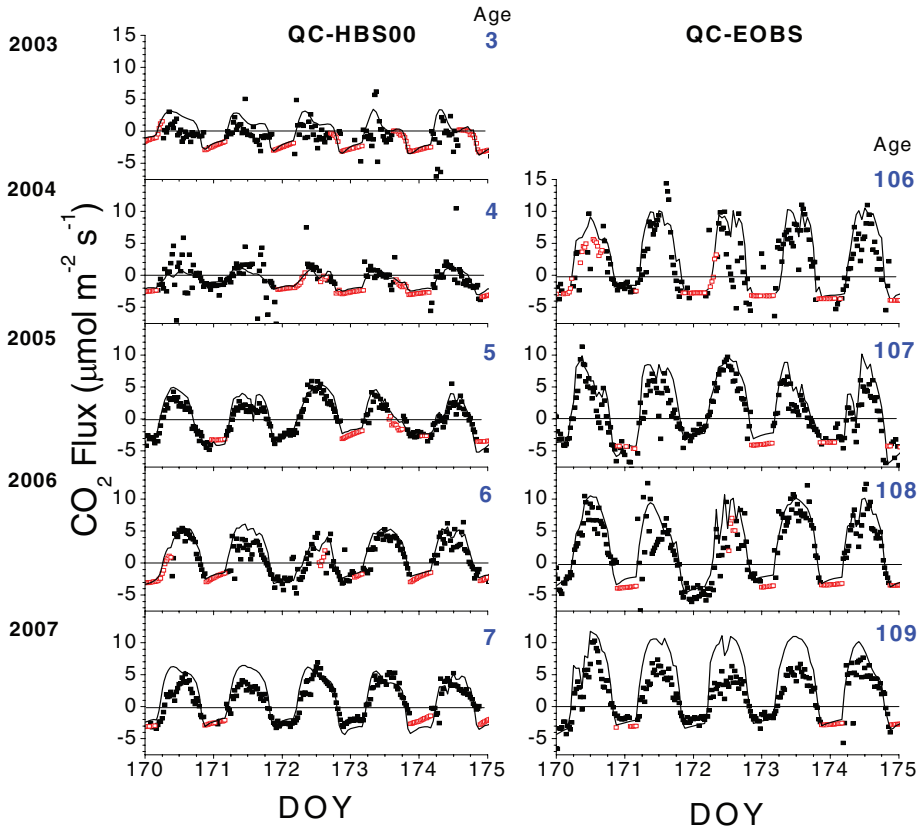

Fig. 3. Hourly CO_2 fluxes measured (closed symbols), gap-filled (open symbols) and modelled (lines) at QC-HBS00 and QC-EOBS during DOY 171–175 from 2003 to 2007. Positive or negative values denote CO_2 influxes or effluxes, respectively.

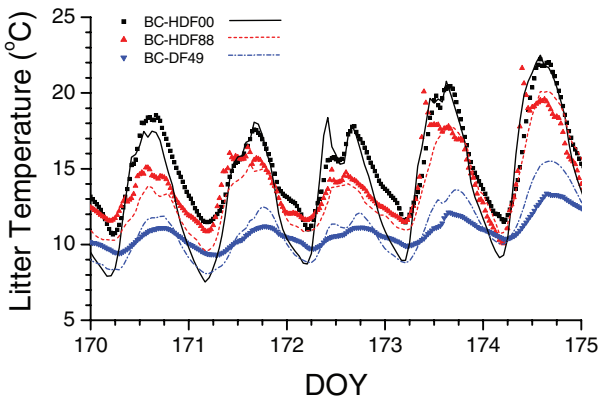

Fig. 4. Soil temperature measured at 2 cm (symbols) and modelled at the bottom of the surface litter layer above the LFH layer (lines) during DOY 171–175 in 2003 at BC-HDF00, BC-HDF88 and BC-DF49.

rises were accelerated by fertilization of the BC chronosequence in 2007, although EC-derived NEP rose less than did modelled NEP because fertilization raised EC-derived R_e at BC-HDF00 and BC-HDF88 and lowered EC-derived GPP at BC-DF49 (Table 4) even though 2007 was a comparatively cool year at these sites (MAT = 7.7 °C).

Table 3. Foliar N concentrations measured and modelled in 2005 at sites regenerating after clearcutting in 2002 (SK-HJP02), 2000 (BC-HDF00,QC-HBS00), 1994 (SK-HJP94), 1988 (BC-HDF88), 1975 (SK-HJP75) and at nearby mature sites (BD-DF49, SK-SOJP, QC-EOBS)

Site	Foliar N	
	Measured (mg N g C^{-1})	Modelled (mg N g C^{-1})
BC-HDF00	22.6 ± 2.8	22.6
BC-HDF88	18.4 ± 2.3	21.2
BC-DF49	18.3 ± 1.2	21.0
SK-HJP02	25.0 ± 2.8	25.8
SK-HJP94	26.4 ± 2.3	14.6
SK-HJP75	22.5 ± 1.6	15.4
SK-SOJP	21.4 ± 0.7	15.2
QC-HBS00	16.4 ± 3.8	16.8
QC-EOBS	15.4 ± 2.7	16.2

4.4. *Changes in ecosystem C stocks with time after clearcutting*

Primary productivity, litterfall and respiration integrated over time in the model led to changes in tree, plant and detrital C

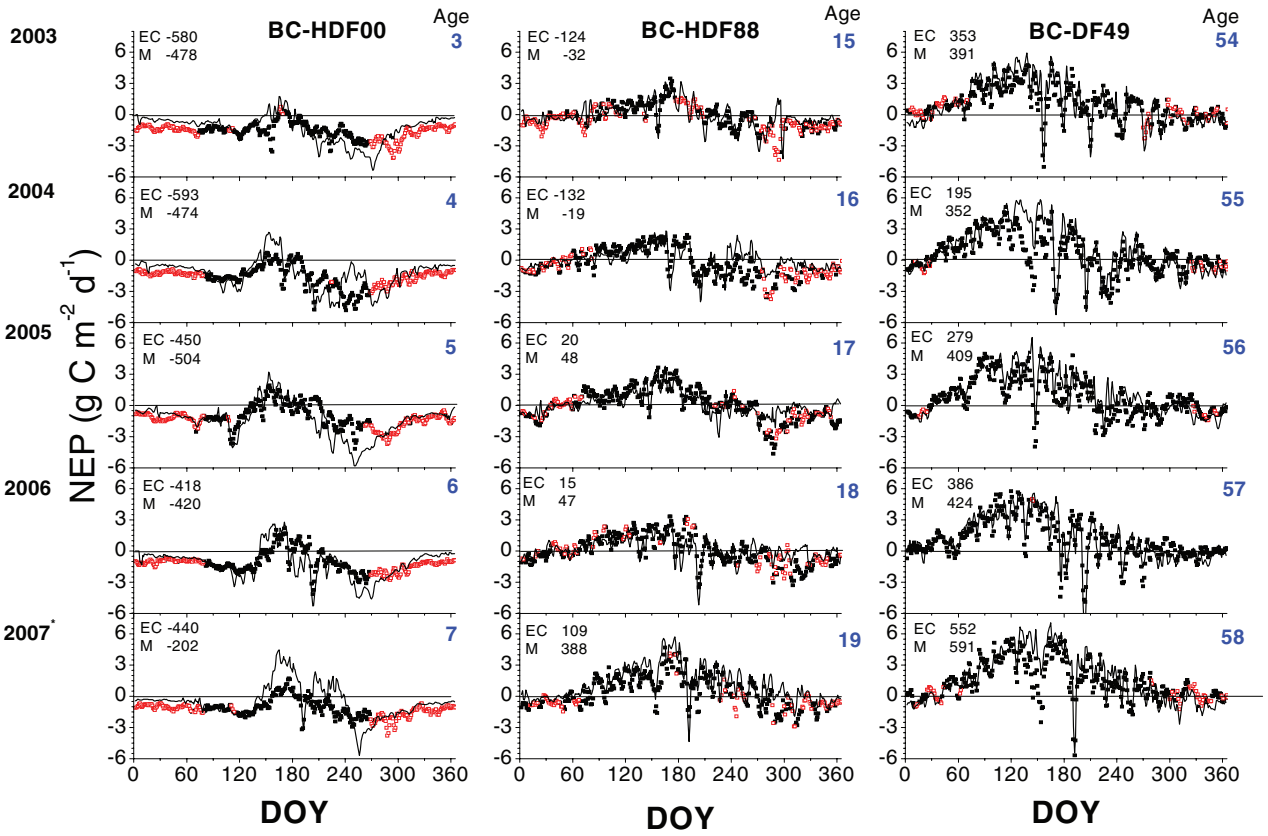

Fig. 5. Daily net ecosystem productivity (NEP) from gap-filled EC measurements (symbols) and modelled (lines) at BC-HDF00, BC-HDF88 and BC-DF49 from 2003 to 2007. Open symbols represent daily NEP consisting of >24 half-hourly gap-filled fluxes. Positive or negative values denote net C uptake or emission, respectively. Numbers in diagrams are total annual NEP from EC and modelled (M) fluxes. BC-HDF00, BC-HDF88 and BC-DF49 stands were fertilized with 6, 20 and 20 g N m^{-2}, respectively as urea in early 2007.

stocks that were compared with similar aboveground C stocks measured in groundplots at each site (Table 5). During model runs, surface WD stocks (excluding standing dead) were replenished by detritus from harvest removals (Table 1), and by ongoing litterfall from living and standing dead phytomass (eq. 13), and depleted by R_h (eq. 3; Table 4). The particularly large WD stock recorded at BC-HDF88 in 2004 was modelled by using a comparatively small harvest removal co-efficient at this site in 1988 (Table 1). Modelled WD stocks tended to exceed the site average groundplot values for all sites in SK and QC (Table 5), Much of the detritus modelled after clearcutting was carried forward from the previous forests (e.g. Fig. 8) and thus in an advanced stage of decomposition, and so may not have been adequately measured in the groundplots. Differences in the definitions of modelled and measured pools could also account for some of the discrepancies.

Plant growth driven by GPP (Table 4) generated live tree (bole, branch and foliage) and understory (foliage and branch) phytomasses during model runs that increased slowly during the first and second decades after clearcutting, but more rapidly thereafter, consistent with the slow but continuous rise in CO_2 influxes modelled and measured with time since clearcutting (Figs 1–3). These phytomasses were, with some exceptions, usually within one standard deviation of the average of measured groundplot values at each site (Table 5), even with common model parameter values used at all sites for all biological properties of each plant functional type. Chronosequences represent a substitution of space for time and although all sites in a chronsequence were modelled as having the same site conditions and pre-clearcut histories, in reality these differed among sites which could further account for the discrepancies between modelled and measured values. Tree wood growth modelled over 100 yr after clearcutting tracked growth curves derived from inventory data for the ecozone in which each chronosequence was located (fig. 12 in Grant et al., 2009a).

4.5. *Changes in net ecosystem productivity with changes in harvest removal*

The effects of fine litter and WD stocks left after clearcutting on the subsequent time courses of R_h, GPP and hence NEP suggest that the harvest practices that determine these stocks

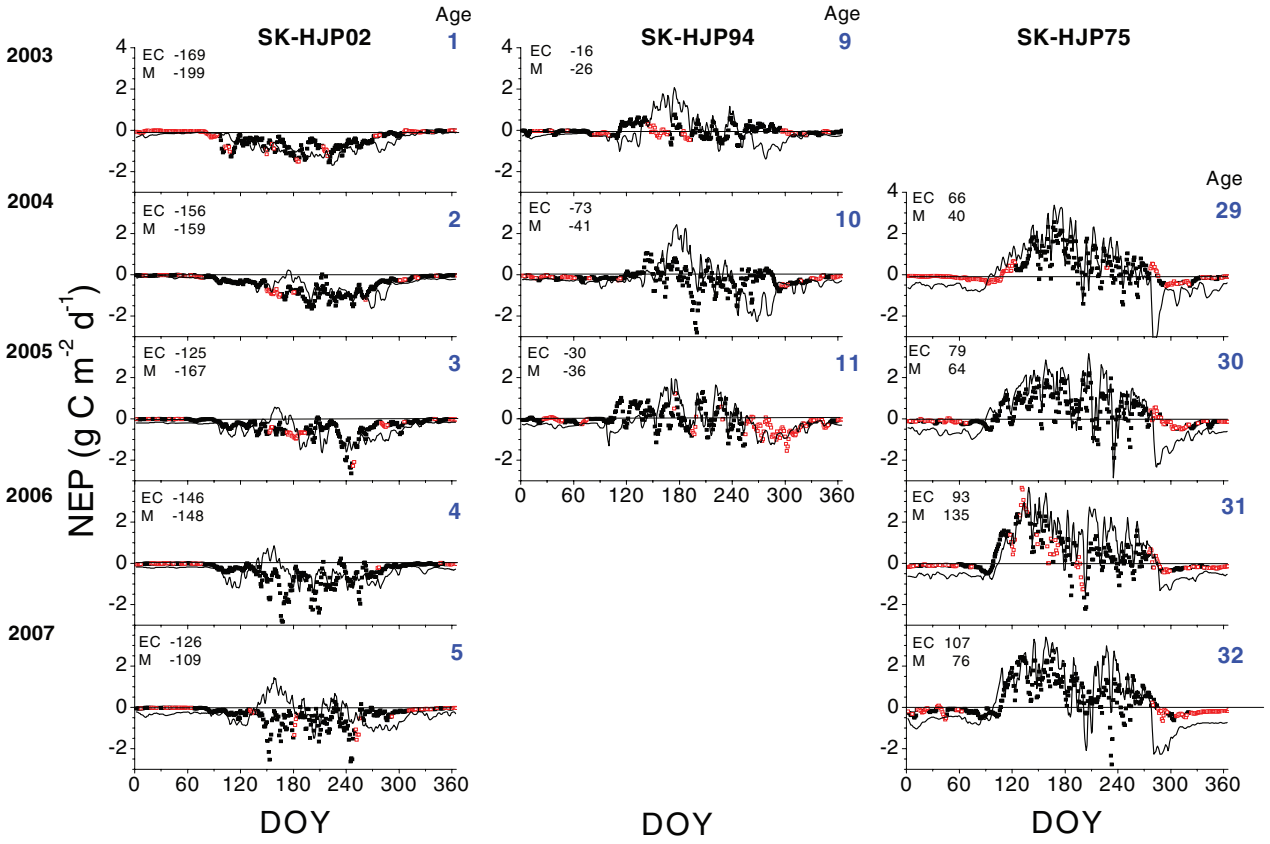

Fig. 6. Daily net ecosystem productivity (NEP) from gap-filled EC measurements (symbols) and modelled (lines) at SK-HJP02, SK-HJP94 and SK-HJP75 from 2003 to 2007. Open symbols represent daily NEP consisting of >24 half-hourly gap-filled fluxes. Positive or negative values denote net C uptake or emission, respectively. Numbers in diagrams are total annual NEP from EC and modelled (M) fluxes.

might affect subsequent forest productivity. In the model, these stocks depended on forest age and productivity before clearcutting, and also on removal coefficients for foliage, other non-woody phytomass, living wood and standing dead wood used to represent the effects of logging practices on forest C distribution (Table 1). The modelled responses of R_h, GPP and NEP to changes in removal coefficients were examined by projecting forest growth for 80 years after clearcutting at BC-HDF88 with removal coefficients for foliage, other non-woody phytomass, and live wood raised by 0.2 and 0.4 from those used in the model tests.

Raising these coefficients reduced the amounts of WD and fine litter left in the model after clearcutting, thereby reducing initial soil + detrital C stocks (Fig. 9a). However these reductions caused slower R_h thereafter (eq. 3), so that soil + detritus C stocks gradually converged towards common values after 80 yr. During the first several years after clearcutting, slower R_h from greater harvest removal caused less immobilization (eq. (8)) of N mineralized during detrital decomposition (eq. 2a), thereby raising N availability for root uptake. However slower R_h from greater harvest removal also caused less asymbiotic N fixation (eqs A26, A27 in Grant et al., 2007b), causing less mineralization of diazotrophic decomposition products, which reduced the gains in N availability from slower immobilization. Raising harvest removal coefficients also reduced the thickness of the surface WD layer, thereby raising temperatures modelled in the forest floor underneath (Fig. 10), as found experimentally by Tan et al. (2009). This warming hastened N mineralization from decomposition (eq. 2a), further raising N availability with greater harvest removal.

The time course of N uptake and assimilation caused foliar N contents in the model to rise during decomposition and mineralization of low C:N fine litter during the first five years after clearcutting (assart effect) (Fig. 9b; Table 3). Foliar N contents then declined during slower decomposition and mineralization of high C:N WD over the following 25 yr, and then rose gradually thereafter during decomposition and mineralization of lower C:N products of litter and WD decomposition. Greater N availability from greater harvest removal hastened early plant N uptake in the model (eq. 17), causing foliar N concentrations to rise slightly during the first 30 years after clearcutting (Fig. 9b). However greater harvest removal caused an eventual reduction in mineralization from decomposition products which caused foliar N concentrations to decline slightly thereafter.

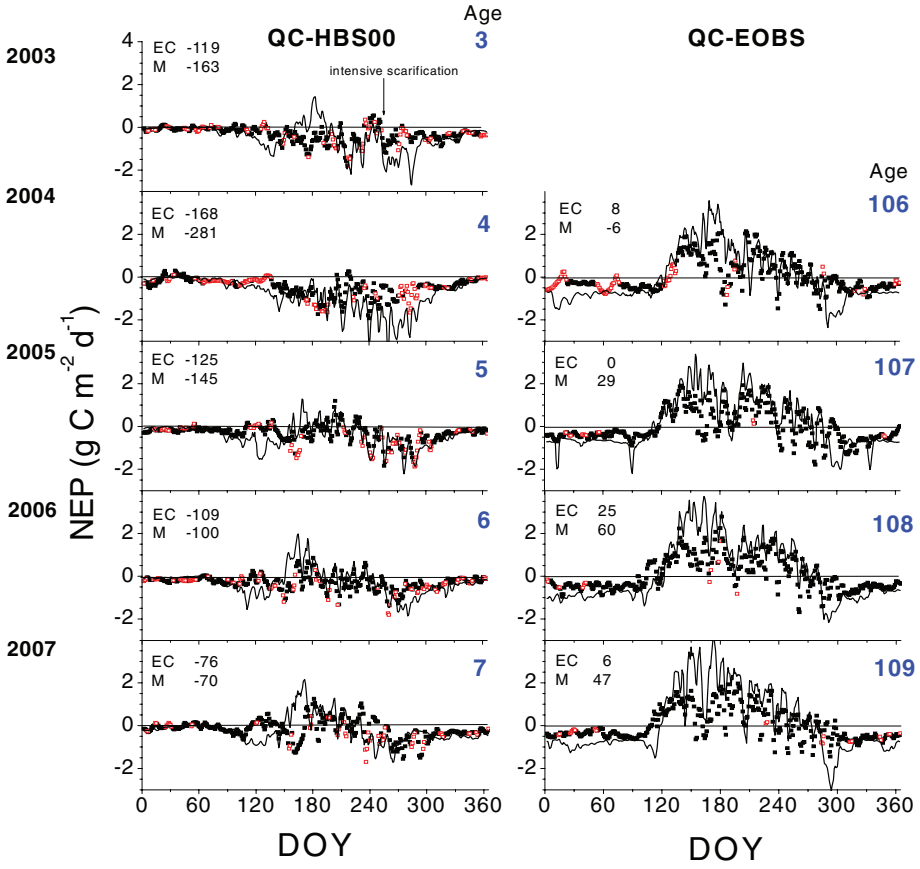

Fig. 7. Daily net ecosystem productivity (NEP) from gap-filled EC measurements (symbols) and modelled (lines) at QC-HBS00 and QC-EOBS from 2003 to 2007. Open symbols represent daily NEP consisting of >24 half-hourly gap-filled fluxes. Positive or negative values denote net C uptake or emission, respectively. Numbers in diagrams are total annual NEP from EC and modelled (M) fluxes.

These changes in foliar N concentrations with harvest removals slightly hastened tree phytomass growth for several decades after clearcutting, but slowed it thereafter, so that net effects of harvest removal on tree phytomass were small (Fig. 9c). Some of the early gain in phytomass modelled with greater harvest removal occurred in the deciduous understory species rather than in the trees. However the modelled understory eventually declined with rising tree LAI, so that most of its C and N stocks were remineralized by 20 yr after clearcutting in all the harvesting treatments. The net effect of greater harvest removal on forest growth in the model thus arose from complex interactions among N transformation processes on N availability that changed over time.

These model results were consistent with findings from other studies that the intensity of wood and litter removal with clearcutting have variable effects on subsequent tree growth. Tan et al. (2009) found that whole tree harvest with slash removal stimulated early lodgepole pine and Douglas-fir growth compared to stem-only harvesting at some BC sites as modelled in our study, but not at others. Olsson and Staaf (1995) found that removal of dense slash layers left from clearcutting boreal pine hastened the early growth of some plant species but not others, although this effect declined as slash decomposed over time, as also modelled in our study. Holcomb (1996) observed that removal of logging slash and forest floors after harvest may reduce productivity at sites with little SOC accumulation, but raise it at sites with greater accumulations, such as modelled at BC-HDF88 in our study. Runs of the FORCYTE-11 process model, tested and calibrated for a Douglas-fir site in the Shawnigan Experimental forest on southern Vancouver Island, predicted that with whole tree harvest, wood production would decline 10–30% after multiple rotations, especially if rotations were short, as accelerated N export of N rich foliage and juvenile wood was greater than the annual N deposition for this site (Trofymow and Sachs, 1991). These variable results in the literature and in our modelling study are consistent with observations that the intensity of wood and litter removal after clearcutting have little effect on C and N pools (Olsson et al., 1996) or on N mineralization rates (Titus et al., 2006) in the soil organic and mineral layers from which most plant N uptake occurs.

By slowing R_h (Fig. 9a) and hastening phytomass growth (Fig. 9c), greater harvest removals caused earlier rises in

Table 4. Annual net ecosystem productivity (NEP), gross primary productivity (GPP), ecosystem respiration (R_e) and heterotrophic respiration (R_h) derived from gap-filled eddy covariance measurements (EC) or modelled from 2001 to 2007 at sites regenerating after clearcutting in 2002 (SK-HJP02), 2000 (BC-HDF00,QC-HBS00), 1994 (SK-HJP94), 1988 (BC-HDF88), 1975 (SK-HJP75) and at nearby mature sites (BD-DF49, SK-SOJP, QC-EOBS)

Site	Year	R_e		R_h		GPP		NEP	
		EC	Model	EC[a]	Model	EC	Model	EC	Model
		g C m^{-2} yr^{-1}							
BC-HDF00	2001	737	710	649	598	166	313	−571	−397
	2002	1013	912	797	745	408	454	−606	−458
	2003	1202	1103	872	862	622	625	−580	−478
	2004	1451	1274	996	954	859	800	−592	−474
	2005	1295	1240	845	946	849	736	−450	−504
	2006	1203	1316	788	951	783	896	−418	−420
	2007†	1566	1141	969	761	1126	939	−440	−202
BC-HDF88	2002	1393	1506	719	819	1271	1409	−121	−97
	2003	1306	1592	680	805	1182	1560	−124	−32
	2004	1589	1747	817	847	1457	1728	−132	−19
	2005	1674	1652	776	791	1694	1700	20	48
	2006	1475	1654	685	750	1490	1701	15	47
	2007†	1686	1677	735	616	1795	2065	109	388
BC-DF49	2001	1667	1766	566	445	2077	2221	410	455
	2002	1675	1864	640	511	1952	2241	277	377
	2003	1724	1852	623	500	2078	2243	353	391
	2004	2078	1897	874	525	2272	2249	195	352
	2005	1970	1826	778	533	2249	2235	279	409
	2006	1726	1827	607	511	2112	2251	386	424
	2007†	1542	1888	432	488	2094	2465	552	577
SK-HJP02	2003	257	291	186	262	88	92	−169	−199
	2004	242	275	196	234	86	116	−156	−159
	2005	250	377	184	301	125	210	−125	−167
	2006	393	408	262	327	247	260	−146	−148
	2007	388	464	249	317	262	355	−126	−109
SK-HJP94	2002	304	488	178	282	237	453	−67	−35
	2003	282	548	140	306	267	522	−16	−26
	2004	488	476	268	280	415	435	−73	−41
	2005	542	543	271	314	512	507	−30	−36
SK-HJP75	2004	494	807	197	363	560	847	66	40
	2005	513	908	199	392	592	972	79	64
	2006	544	975	206	390	637	1110	93	135
	2007	527	908	191	392	634	1015	107	76
SK-SOJP	2001	605	921	262	315	648	1021	42	100
	2002	544	866	263	324	529	875	−15	9
	2003	528	864	241	313	542	876	14	12
	2004	556	856	259	375	560	903	4	47
	2005	558	887	243	358	594	949	36	62
	2006	605	925	267	340	638	1047	33	122
	2007	536	932	215	359	605	996	69	64
QC-HBS00	2002	393	486	257	380	256	297	−137	−189
	2003	436	480	268	363	317	317	−119	−163
	2004	442	543	296	440	275	262	−168	−281

Table 4. Continued

Site	Year	R_e		R_h		GPP		NEP	
		EC	Model	EC[a]	Model	EC	Model	EC	Model
		g C m^{-2} yr^{-1}							
	2005	485	558	294	394	361	413	−125	−145
	2006	504	501	294	339	396	401	−109	−100
	2007	502	398	276	263	426	328	−76	−70
QC-EOBS	2004	582	774	269	327	590	768	8	−6
	2005	677	916	318	378	678	945	1	29
	2006	633	870	285	356	657	930	25	60
	2007	591	853	275	351	597	900	6	47

Notes: BC-HDF00, BC-HDF88 and BC-DF49 stands were fertilized with 6, 20 and 20 g N m^{-2} as urea in early 2007.

[a]Estimated as $R_e - 0.53 \times$ GPP from Waring and Running (1998).

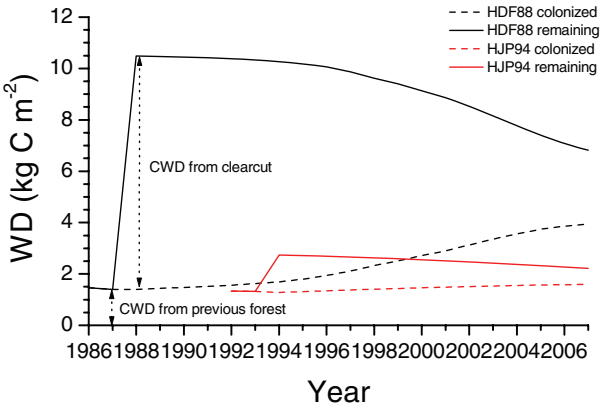

Fig. 8. Colonized and total woody debris (WD) (= S_C and $S_C + S_C'$ in eq. 10) remaining in the model to 2007 after clearcutting at BC-HDF88 in 1988 and SK-HJP94 in 1994.

modelled NEP, allowing C neutrality to be reached several years sooner (Fig. 9d). This model response was consistent with that of an empirical model based on inventories in post-disturbance chronosequences of Douglas fir-dominated forests by Janisch and Harmon (2002). In their model, greater wood removal reduced the early decline in NEP and hastened the subsequent rise in NEP to C neutrality after clearcutting. However NEP in *ecosys* converged to similar values during later forest regeneration more than 30 yr after the different harvest removals (Fig. 9d), in contrast to NEP predicted during regeneration by Janisch and Harmon (2002) which rose less and remained lower with greater removal. This convergence in *ecosys* occurred because removal effects on C stocks in soil + detritus (Fig. 9a) and trees (Fig. 9c) both diminished over time, and so only affected NEP during the first three decades after clearcutting. Model results collectively indicated that greater harvest removal at BC-HDF88 would have a large effect on NEP within 30 yr after clearcutting (Fig. 9d), but only a limited effect thereafter.

Raising removal coefficients by 0.2 and 0.4 from those used in model testing caused harvest removals to increase by 3645 and 7290 g C m^{-2}, respectively. These increased removals caused reductions in ecosystem C stocks (living + standing dead trees, WD, fine litter, humus, and losses through DOC + DIC export) of 541 and 1188 g C m^{-2}, respectively after an 80-yr harvest cycle, or about 15% of the increased removals. These losses represented the cost of the removals to ecosystem C stocks at the following harvest.

5. Discussion

5.1. *Controls on the time courses of respiration and productivity after clearcutting*

The time courses of NEP modelled and measured after clearcutting at the three chronosequences in this study arose from different time courses of respiration and primary productivity. Modelled and EC-derived R_h rose with higher detritus stocks (Table 5) and temperatures (e.g. Fig. 4) over 2–7 yr of measurement in the recently clearcut sites at BC-HDF00, SK-HJP02 and QC-HBS00, remained high in the 10–20-year-old post-clearcut sites at BC-HDF88 and SK-HJP94, then declined and eventually stabilized after more than 20 yr with declining detritus stocks and temperatures and rising litterfall and mortality in the older forest sites at BC-DF49 and SK-HJP75 (Table 4). Some interannual variability was superimposed on this trend, such as higher values modelled and measured during 2004, a year with a particularly warm summer at the BC chronosequence, and from 2004 to 2006, during which warming occurred at the SK and QC chronosequences (Grant et al., 2009a). This time course of R_h with time since clearcutting in the model appeared

Table 5. Above-ground C stocks measured (simple average ± standard deviation for all groundplots) and modelled at sites regenerating after clearcutting in 2002 (SK-HJP02), 2000 (BC-HDF00, QC-HBS00), 1994 (SK-HJP94), 1988 (BC-HDF88), 1975 (SK-HJP75) and in nearby older forest sites (BC-DF49, SK-SOJP, QC-EOBS)

Site	C Stock					
	Live overstory		Live understory[a]		Down woody debris	
	Measured (g C m^{-2})	Modelled (g C m^{-2})	Measured (g C m^{-2})	Modelled (g C m^{-2})	Measured (g C m^{-2})	Modelled (g C m^{-2})
BC-HDF00 (2002)[b]	21 ± 53	1	134 ± 48	99	3500 ± 3166	5971
BC-HDF88 (2002)[b]	826 ± 365	825	306 ± 127	210	7943 ± 2291	8523
BC-DF49 (2002)[b]	15801± 3527	16231	34 ± 16	0	5413 ± 2402	3660
SK-HJP02 (2004)[c]	0 ± 0	4	29 ± 18	44	894 ± 135	2972
SK-HJP94 (2004)[c]	169 ± 49	168	11 ± 9	84	576 ± 108	2380
SK-HJP75 (2004)[c]	2080 ± 88	2009	32 ± 7	33	360 ± 92 run244q02	996
SK-SOJP (2004)[c]	5155 ± 927	3761	55 ± 21	64	298 ± 90	1308
QC-HBS00 (2005)[d]	33	3	64	120		1951
QC-EOBS (2003)[e]	4456	5949	N/A	90	800	2082

Notes: Live overstory includes foliage, branches and bole; woody debris includes coarse, medium and small size classes >1 cm; excludes stumps, standing dead, fine woody debris <1cm and surface LFH layers.

[a]Includes mosses at BC and QC sites, excludes mosses at SK sites.

[b]Trofymow, J.A. (2008) FCRN DIS at http://fluxnet.ccrp.ec.gc.ca

[c]Barr, A.G. (2008) FCRN DIS at http://fluxnet.ccrp.ec.gc.ca

[d]Giasson et al. (2006)

[e]Margolis, H.A. 2008. FCRN DIS at http://fluxnet.ccrp.ec.gc.ca

consistent with that from field studies. Martin et al. (2002) found that decomposition rates measured in a post-clearcut silver fir-western hemlock chronosequence in BC rose during the first 6 yr, and declined thereafter. Kolari et al. (2004) found that soil respiration R_s measured in a post-clearcut pine chronosequence in southern Finland was highest in a 12-year-old stand and lower in both younger and older stands. However in some cases drier surface conditions were found to slow decomposition at exposed clearcut sites in post-harvest chronosequences of Douglas-fir on southern Vancouver Island (Trofymow, 1998; Addison et al., 2003). Declining contributions of R_h to R_e more than 5 yr after clearcutting may therefore be a general phenomenon, causing R_e to rise little with forest age more than 20 yr after clearcutting (Table 4).

In the model, the time course of R_h was simulated with a function for microbial colonization of WD and fine litter (eq. 10) that simulated gradual rises in decomposition and hence R_h from new detritus for several years after clearcutting followed by gradual declines (Fig. 8), as frequently observed in field studies (e.g. Mäkinen et al., 2006; Montes and Cañellas, 2006). The time course of R_h in the model caused NEP to remain negative but stable for the first decade after clearcutting, and to rise only gradually during the second decade. This time course of NEP generally matched that of the EC-derived NEP (Figs. 1–3, 5–7; Table 4). However this time course could not be modelled from simple first-order functions of the amounts of WD and fine litter left after clearcutting as done in many empirical models, which can give only declining R_h and hence rising NEP with time following clearcutting.

In contrast to the time course of R_e as driven by R_h, that of GPP indicated a gradual but continuous rise from reseeding to maturity (Figs 1–3) which drove the gradual rise in NEP beginning several years after clearcutting (Table 4). The rate at which GPP rose in the model was constrained by low foliar N concentrations (Table 3), the time course of which was similar to that measured in other field studies. Bradley et al. (2002) found that foliar N concentrations declined from 24.4 to 17.6 and 16.3 mg N g C^{-1} (assuming needles are 50% C) in 4-, 7- and 11-year-old stands, respectively in a post-clearcut chronosequence of silver fir-western hemlock in coastal BC. Bradley et al. (2002) attributed this decline to measurements of mineral N availability that rose to maximum values 4–5 yr after clearcutting, and declined thereafter. This time course of mineral N availability was found to follow that of slash decomposition after clearcutting as measured by Martin et al. (2002) and modelled in this study (Table 4).

The time course of foliar N concentrations was hypothesized in the model to arise from the time courses of decomposition (eqs 1, 2; Fig. 8), microbial growth (eqs 7, 9), colonization (eq. 10), nutrient mineralization versus immobilization (eq. 8) and asymbiotic N_2 fixation (eqs A26, A27 in Grant et al., 2007b) in WD and fine litter complexes with, respectively higher versus lower C:N ratios, and lower versus higher specific decomposition rates. These processes controlled the time course of soil

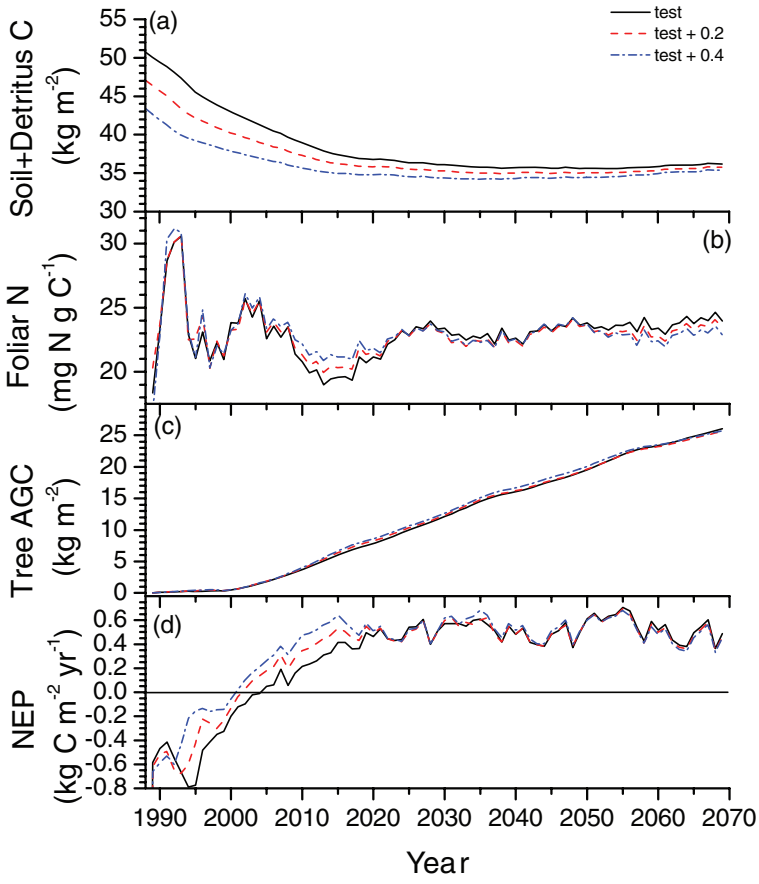

Fig. 9. (a) Total soil + detritus C, (b) foliar N content, (c) Douglas-fir + understory live biomass C and (d) net ecosystem productivity (NEP) modelled over 80 years (normal harvesting cycle) after clearcutting at BC-HDF88 with clearcut removal coefficients for foliage, other non-woody phytomass, living and standing dead wood used in the model tests (Table 1), and raised by 0.2 and 0.4.

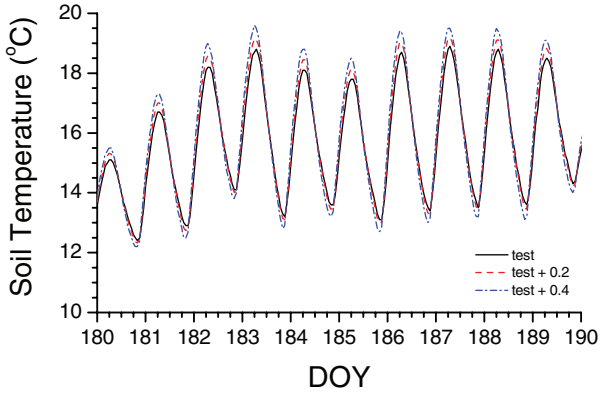

Fig. 10. Soil temperatures modelled at the bottom of the surface litter layer above the LFH layer at BC-HDF88 during DOY 180–190 in 1991 after raising clearcut removal coefficients for foliage, other non-woody phytomass, living and standing dead wood by 0.2 and 0.4 from those used in model testing.

mineral N concentrations that drove root and mycorrhizal N uptake (eq. 17) and plant N assimilation (eq. 19; Table 3) that in turn drove growth in root and mycorrhizal lengths (eq. 16) and in leaf areas (eq. 20), and hence rises in N uptake (eq. 17) and GPP (eq. A7 in Grant et al., 2010).

Interactions among these processes generated time courses for long-term projections of C accumulation in pioneer shrubs and dominant trees that reproduced the Chapman–Richards functions used to estimate slow early growth in empirical models (e.g. Janisch and Harmon, 2002; Taylor et al., 2005; Kurz et al., 2009) under diverse site conditions (Table 5; Grant et al., 2009a). When the time courses of GPP that drove C accumulation were combined with those of R_e as driven by R_h, the model was able to generate different time courses of NEP among the three post-clearcut chronosequences that were consistent with EC-derived values, without resorting to site- and species-specific parametrizations. Thus the more productive temperate BC sites with greater WD stocks left by clearcutting (Table 5) had greater R_h and lower NEP for several years after clearcutting, but attained greater GPP and hence NEP during later years than did the less productive boreal sites in SK and QC (Table 4).

Continuous EC measurements of CO_2 fluxes along diverse post-clearcut chronosequences have improved constraints to testing a process-based model of decomposition and regrowth. This testing has enabled a robust simulation of post-harvest changes in forest C stocks, allowing the model to be used in life-cycle studies of forest C following harvest (e.g. Fig. 9) without the need for site-specific parameterization.

6. Acknowledgments

Computing facilities for *ecosys* were provided by the University of Alberta and by Cybera, a corporation managing cyberinfrastructure-related technologies in collaboration with academic and industry partners. Funding for this study was provided by a CFCAS grant to the Canadian Carbon Program (CCP), National Sciences and Engineering Research Council of Canada (NSERC) network and strategic grants to the University of British Columbia (UBC) and by the Natural Resource Canada PERD program. We thank Bob Ferris, Gurp Thandi, Colin Ferster, Mark Gillis and Frank Eichel of the Canadian Forest Service (CFS) and staff of B.A. Blackwell and Associates for their help collecting and processing National Forest Inventory-style ground plot data for the BC coastal sites.

Appendix A: Values of key parameters used to model decomposition and growth in *ecosys*

Variable	Definition	Units	Equation	Value	Reference
C_N, C_P	Maximum ratio of M_N or M_P to M_C	g N or P g C^{-1}	(3, 8)	0.22 and 0.13 (N), 0.022 and 0.013 (P) for j = labile and resistant	Grant et al. (1993a,b)
D_{SC}	Specific decomposition rate of S_C by M_C at 25°C and saturating [S_C]	g C g C^{-1} h^{-1}	(1)	1.0 (protein), 1.0 (carbo.), 0.15 (cellulose), 0.025 (lignin)	Grant et al. (1993a,b)
E_n	Energy requirement for growth of M_C	kJ g C^{-1}	(5)	25	
F	Fraction of microbial growth allocated to kinetic components of M_C	–	(7, 9)	0.55 (labile), 0.45 (resistant)	Grant et al. (1993a,b)
K_{iD}	Inhibition constant for M_C on S_C	g C m^{-3}	(1)	25	Grant et al. (1993a,b)
K_{iS}	Inhibition constant for colonization of detritus by growth of M_C	–	(10)	0.5	
$K_{i\sigma N}$	Inhibition constant for $\sigma_{Ci,j}$ versus $\sigma_{Ni,j}$	g C g N^{-1}	(19)	100	Grant (1998)
$K_{i\sigma P}$	Inhibition constant for $\sigma_{Ci,j}$ versus $\sigma_{Pi,j}$	g C g P^{-1}	(19)	1000	Grant (1998)
K_{mD}	Half-saturation constant for D_{SC} of S_C	g C Mg^{-1}	(1)	8750 (surface CWL), 750 (subsurface CWL), 225 (surface fine), 75(subsurface fine)	
K_{mQ}	Half-saturation constant for R_h on [Q_C]	g C m^{-3}	(3)	36	Grant et al. (1993a,b)
K_{NH_4}	Half-saturation constant for NH_4^+ uptake at microbial, root or mycorrhizal surfaces	g N m^{-3}	(8, 17)	0.40	Barber and Silberbush, 1984
[$NH_4^+{}_{mn}$]	Concentration of NH_4^+ at microbial, root or mycorrizal surfaces below which $U_{NH_4} = 0$	g N m^{-3}	(8, 17)	0.0125	Barber and Silberbush, 1984
R_c'	Specific respiration of σ_C at 25 °C	g C g C^{-1} h^{-1}	(12)	0.015	
R_h	Specific heterotrophic respiration of M_C under nonlimiting [Q_C], O_2, nutrients, at 25°C	g C g C^{-1} h^{-1}	(3)	0.125	Shields et al. (1973)
U'_{NH_4}	Maximum U_{NH_4} by root, mycorrhizal and microbial surfaces at 25 °C and non-limiting NH_4^+	g N m^{-2} h^{-1}	(8, 17)	5.0×10^{-3}	Barber and Silberbush, 1984
Y_g	Fraction of σ_C used for growth expended as R_g	g C g C^{-1}	(15, 18)	0.28 (leaf), 0.24 (root and other non-foliar), 0.20 (wood)	Waring and Running (1998)
ΔG	Energy yield of C oxidation and O_2 reduction	kJ g C^{-1}	(5)	37.5	
α	Growth in leaf area per unit growth in leaf mass	m^2 g^{-3}	(20)	0.0083 (conifer), 0.0125 (deciduous)	Grant and Hesketh, 1992)
β	Specific colonization of detritus by growth of M_C	g C g C^{-1} h^{-1}	(10)	2.0	
θ_P	Root or mycorrhizal porosity	m3 m-3	(16)	0.25	Grant (1998)
ρ	Density of root biomass	g g−1	(16)	0.125	Grant (1998)
ψ_t'	Canopy turgor potential below which growth = 0	MPa	(14, 19)	0.1	

References

Aakala, T., Kuuluvainen, T., De Grandpré, L. and Gauthier, S. 2007. Trees dying standing in the northeastern boreal old-growth forests of Quebec: spatial patterns, rates, and temporal variation. *Can. J. For. Res.* **37**, 50–61.

Addison, J., Trofymow, J. and Marshall, V. G. 2003. Functional role of *Collembola* in decomposition in coastal temperate rainforests. *Appl. Soil Ecol.* **24**, 247–261.

Barber, S. A. and Silberbush, M. 1984. Plant root morphology and nutrient uptake. In: *Roots, Nutrient and Water Influx, and Plant Growth* (eds S. A. Barber and D. R. Bouldin), Amer. Soc. Agron. Spec. Publ. no. 49, Madison, WI, 65–87.

Barr, A. G., Black, T. A., Hogg, E. H., Kljun, N., Morgenstern, K. and co-authors. 2004. Inter-annual variability in the leaf area index of a boreal aspen-hazelnut forest in relation to net ecosystem production. *Agric. For. Meteorol.* **126**, 237–255.

Bergeron, O., Margolis, H. A., Coursolle, C. and Giasson, M.-A. 2008. How does forest harvest influence carbon dioxide fluxes of black spruce ecosystems in eastern North America? *Agric. For. Meteorol.* **148**, 537–548.

Bradley, R. L., Kimmins, J. P. and Martin, W. L. 2002. Post-clearcutting chronosequence in the B.C. Coastal Western Hemlock Zone. II. Tracking the assart flush. *J. Sust. For.* **14**, 23–43.

Chen, B., Black, T. A., Coops, N. C., Hilker, T., Trofymow, J. A. and co-authors. 2009. Assessing tower flux footprint climatology and scaling between remotely sensed and eddy covariance measurements. *Bound.-Layer Meteorol.* **130**, 137–167.

Cohen, W. B., Harmon, M. E., Wallin, D. O. and Fiorella, M. 1996. Two decades of carbon fluxes from forests of the Pacific northwest. *Biosci*. **46**, 836–844.

Diochon A., Kellman, L. and Beltrami, H. 2009. Looking deeper: An investigation of soil carbon losses following harvesting from a managed northeastern red spruce (*Picea rubens* Sarg.) forest chronosequence. *Forest Ecol. Manage*. **257**, 413–420.

Edmonds, R. L. and Hsiang, T. 1987. Forest floor and soil influence on response of Douglas-fir to urea. *Soil Sci. Soc. Am. J.* **51**, 1332–1337.

Farquhar G. D., von Caemmerer, S. and Berry, J. A. 1980. A biochemical model of photosynthetic CO_2 assimilation in leaves of C3 species. *Planta* **149**, 78–90.

Giasson, M.-A., Coursolle, C. and Margolis, H. A. 2006. Ecosystem level CO_2 fluxes from a boreal cutover in eastern Canada before and after scarification. *Agric. For. Meteorol.* **140**, 23–40.

Grant, R. F. 1998. Simulation in *ecosys* of root growth response to contrasting soil water and nitrogen. *Ecol. Modelling* **107**, 237–264.

Grant, R. F. 2004. Modelling topographic effects on net ecosystem productivity of boreal black spruce forests. *Tree Physiol*. **24**, 1–18.

Grant, R. F. and Hesketh, J. D. 1992. Canopy structure of maize *(Zea mays L.)* at different populations: simulation and experimental verification. *Biotronics* **21**, 11–24.

Grant, R. F., Juma, N. G. and McGill, W. B. 1993a. Simulation of carbon and nitrogen transformations in soils. I: mineralization. *Soil Biol. Biochem.* **27**, 1317–1329.

Grant, R. F., Juma, N. G. and McGill, W. B. 1993b. Simulation of carbon and nitrogen transformations in soils. II: microbial biomass and metabolic products. *Soil Biol. Biochem.* **27**, 1331–1338.

Grant, R. F., Barr, A. G., Black, T. A., Iwashita, I., Kidson, J. and co-authors. 2007a. Net ecosystem productivity of boreal jack pine stands regenerating from clearcutting under current and future climates. *Global Change Biol*. **13**, 1423–1440.

Grant, R. F., Black, T. A., Humphreys, E. R., and Morgenstern, K. 2007b. Changes in net ecosystem productivity with forest age following clearcutting of a coastal Douglas fir forest: testing a mathematical model with eddy covariance measurements along a forest chronosequence. *Tree Physiol*. **27**, 115–131.

Grant, R. F., Margolis, H. A., Barr, A. G., Black, T. A., Dunn, A. L. and co-authors. 2008. Changes in net ecosystem productivity of boreal black spruce stands in response to changes in temperature at diurnal and seasonal time scales. *Tree Physiol.* **29**, 1–17.

Grant, R. F., Barr, A. G., Black, T. A., Margolis, H. A., Dunn and co-authors. 2009a. Interannual variation in net ecosystem productivity of Canadian forests as affected by regional weather patterns—a Fluxnet-Canada synthesis. *Agric. For. Meteorol.* 149(1), 2022–2039.

Grant, R. F., Hutyra, L. R., de Oliveira, R. C., Munger, J. W., Saleska, S. R. and co-authors. 2009b. Modelling the carbon balance of Amazonian rainforests: resolving ecological controls on net ecosystem productivity. *Ecol. Appl.* **79**(3), 445–4638.

Grant, R. F., Jassal, R. S. and Black, T. A. 2010. Changes in net CO_2 and N_2O exchange with fertilization of Douglas fir: mathematical modelling in *ecosys*. *J. Geophys. Res.*, doi:10.1029/2009JG001094.

Grenon, F., Bradley, R. L., Joanisse, G., Titus B. D. and Prescott, C. E. 2009. Mineral N availability for conifer growth following clearcutting: responsive versus non-responsive ecosystems. *Forest Ecol. Manage.* **188**, 305–316.

Grier, G. C. 1978. A *Tsuga heterophylla—Picea sitchensis* ecosystem of coastal Oregon: decomposition and nutrient balances of fallen logs. *Can. J. For. Res*. **8**(2), 198–206.

Harmon, M. E., Franklin, J. F., Swanson, F. J., Sollins, P., Gregory, S. V. and co-authors. 1986. Ecology of coarse woody debris in temperate ecosystems. *Adv. Ecol. Res.* **15**, 133–302.

Holcomb, R. W. 1996. *The long-term soil productivity study in British Columbia*. FRDA Report 256, BC Ministry of Forests, Victoria, BC, Canada.

Holland, E. A., Dentener, F. J., Braswell B. H. and Sulzman, J. M. 1999. Contemporary and pre-industrial global reactive nitrogen budgets. *Biogeochemistry* **46**, 7–43.

Hopmans P. and Chappell, H. N. 1994. Growth response of young, thinned Douglas-fir stands to nitrogen fertilizer in relation to soil properties and tree nutrition. *Can. J. For. Res.* **24**(8), 1684–1688.

Humphreys, E. R., Black, T. A., Morgenstern, K., Li, Z. and Nesic, Z. 2005. Net ecosystem production of a Douglas-fir stand for 3 years following clearcut harvesting. *Global Change Biol*.**11**, 450–464.

Howard, E. A., Gower, S. T., Foley, J. A. and Kucharik, C. J. 2004. Effects of logging on carbon dynamics of a jack pine forest in Saskatchewan, Canada. *Global Change Biol.* **10**, 1–18.

Janisch, J. E. and Harmon, M. E. 2002. Successional changes in live and dead wood carbon stores: implications for net ecosystem productivity. *Tree Physiol*. **22**, 77–89.

Jassal, R. S., Black, T. A., Cai, T., Morgenstern, K., Li, Z. and co-authors. 2007. Components of ecosystem respiration and an estimate of net primary productivity of an intermediate-aged Douglas-fir stand. *Agric. For. Meteorol.* **144**, 44–57.

Jassal, R. S., Black, T. A., Spittlehouse, D. L., Brümmer, C. and Nesic, Z. 2009. Evapotranspiration and water use efficiency in

different-aged Pacific Northwest Douglas-fir stands. *Agric. For. Meteorol.* **149**, 1168–1178.

Johnson, D. W. and Curtis, P. S. 2001. Effects of forest management on soil C and N storage: meta analysis. *For. Ecol. Manage.* **140**, 227–238.

Kolari, P., Pumpanen, J., Rannik, U., Ilvesniemi, H., Hari, P. and co-authors. 2004. Carbon balance of different aged Scots pine forests in Southern Finland. *Global Change Biol*. **10**, 1106–1119.

Kimmins, J. P. 2004. *Forest Ecology: A Foundation For Sustainable Forest Management and Environmental Ethics in Forestry* 3rd Edition. Pearson Prentice Hall, NJ.

Kurz, W. A. and Apps, M. J. 1999. A 70 year retrospective analysis of carbon fluxes in the Canadian forest sector. *Ecol. Appl.* **9**, 526–547.

Kurz, W. A., Dymond, C. C., White, T. M., Stinson, G., Shaw and co-authors. 2009. CBM-CFS3: A model of carbon-dynamics in forestry and land-use change implementing IPCC standards. *Ecol. Model.* **220**, 480–504.

Litvak, M., Miller, S., Wofsy, S. C. and Goulden, M. 2003. Effect of stand age on whole system CO_2 exchange in the Canadian boreal forest. *J. Geophys. Res.* **108**(D3), 8225. doi:10.1029/2001JDD000854.

Mäkinen, H., Hynynen, J., Siitonen, J. and Sievänen, R. 2006. Predicting the decomposition of Scots pine, Norway spruce, and birch stems in Finland. *Ecol. Appl.* **16**, 1865–1879.

Martin, W. L., Bradley, R. L. and Kimmins, J. P. 2002. Post-clearcutting chronosequence in the B.C. coastal western hemlock zone: I. Changes in forest floor mass and N storage. *J. Sust. For.* **14**, 1–22.

Melin, Y., Petersson, H. and Nordfjell, T. 2009. Decomposition of stump and root systems of Norway spruce in Sweden—A modelling approach. *For. Ecol. Manage.* **257**, 1445–1451.

Meteorological Service of Canada. 2004. *Canadian Acid Deposition Science assessment*. Environment Canada, Ottawa, ON.

Mkhabela, M. S., Amiro, B. D., Barr, A. G., Black, T. A., Hawthorne, I. and co-authors. 2009. Comparison of carbon dynamics and water use efficiency following fire and harvesting in Canadian boreal forests. *Agric. For. Meteorol.* **149**, 783–794.

Montes, F. and Cañellas, I. 2006. Modelling coarse woody debris dynamics in even-aged Scots pine forests. *For. Ecol. Manage.* **221**, 220–232.

Müller-Using S. and Bartsch, N. 2009. Decay dynamic of coarse and fine woody debris of a beech (*Fagus sylvatica* L.) forest in Central Germany. *Eur. J. For. Res.* **128**, 287–296.

Næsset, E. 1999. Decomposition rate constants of *Picea abies* logs in southeastern Norway. *Can. J. For. Res*. **29**, 372–381.

National Forest Inventory Taskforce. 2008. Canada's National Forest Inventory Ground Sampling Guidelines: specification for ongoing measurements. Canadian Council of Forest Ministers. Retrieved from: https://nfi.nfis.org/documentation/ground_plot/Gp_guidelines_v4.1.pdf. Accessed in 2008.

Olsson, B. A. and Staaf, H. 1995. Influence of harvesting logging residues on ground vegetation in coniferous forests. *J. Appl. Ecol.* **32**, 640–654.

Olsson, B. A., Staaf, H., Lundkvist, H., Bengtsson, J. and Rosén, K. 1996. Carbon and nitrogen coniferous forest soils after clearfelling and harvests of different intensity. *For. Ecol. Manage.* **82**, 19–32.

Ranius, T., Kindvall, O., Kruys, N. and Jonsson, B. G. 2003. Modelling dead wood in Norway spruce stands subject to different mangement regimes. *For. Ecol. Manage.* **182**, 13–29.

Richardson, A. D., Hollinger, D. Y., Burba, G. G., Davis, K. J., Flanagan, L. B. and co-authors. 2006. A multi-site analysis of random error in tower-based measurements of carbon and energy fluxes. *Agric. For. Meteorol*. **136**, 1–18.

Shields J. A., Paul, E. A., Lowe, W. E. and Parkinson, D. 1973. Turnover of microbial tissue in soil under field conditions. *Soil Biol. Biochem.* **5**, 753–764.

Schimel, J. P. and Firestone, M. K. 1989. Nitrogen incorporation and flow through a coniferous forest soil profile. *Soil Sci. Soc. Am. J.* **533**, 779–784.

Schulze, E. -D., LLoyd, J., Kelliher, F. M., Wirth, C., Rebmann and co-authors. 1999. Productivity of forests in the Eurosiberian boreal region and their potential to act as a carbon sink – a synthesis. *Global Change Biol*. **5**, 703–722.

Schwalm, C. R., Black, T. A., Morgenstern, K. and Humphreys, E. R. 2007. A method for deriving net primary productivity and component respiratory fluxes from tower-based eddy covariance data: a case study using a 17-year data record from a Douglas-fir chronosequence. *Global Change Biol.* **13**, 370–385.

Shorohova, E., Kapitsa, E. and Vanha-Majamaa, I. 2008. Decomposition of stumps in a chronosequence after clear-felling vs. clear-felling with prescribed burning in a southern boreal forest in Finland. *For. Ecol. Manage.* **255**, 3606–3612.

Siitonen, J., Martikainen, P., Punttila, P. and Rauh, J. 2000. Coarse woody debris and stand characteristics in mature managed and old-growth boreal mesic forests in southern Finland. *For. Ecol. Manage.* **128**, 211–225.

Tan, X., Curran, M., Chang, S. and Maynard, D. 2009. Early growth responses of Lodgepole pine and Douglas-fir to soil compaction. *For. Sci.* **55**, 210–220.

Taylor, A. R., Wang, J. R. and Chen, H. Y. H. 2005. Carbon storage in a chronosequence of red spruce (*Picea rubens*) forests in central Nova Scotia, Canada. *Can. J. For. Res.* **37**, 2260–2269.

Titus, B. D., Prescott, C. E., Maynard, D. G., Mitchell, A. K., Bradley, R. L. and co-authors. 2006. Post-harvest nitrogen cycling in clearcut and alternative silvicultural systems in a montane forest in coastal British Columbia. *For. Chron.* **82**, 844–859.

Trofymow, J. A. 1998. Detrital carbon fluxes and microbial activity in successional Douglas-fir forests. *Northwest Sci*. **72**(2), 51–53.

Trofymow, J. A., Moore, T. R., Titus, B., Prescott, C., Morrison, I. and co-authors. 2002. Rates of litter decomposition over 6 years in Canadian forests: influence of litter quality and climate. *Can. J. For. Res.* **32**, 789–804.

Trofymow, J. A. and Sachs, D. 1991. FORCYTE-11 and intensive management of Douglas-fir: Examination of some of the model's short- and long- term predictions of biomass production. In: *Proceedings of the Fifth Annual Forestry Canada Modeling Working Group Workshop* (H. Grewal (compiler)) Dec 13–14, 1990, Kananaskis Centre. Canadian Forest Service, Nor. For. Cen., Edmonton, AB, 38–57.

Trofymow, J. A., Stinson, G., and Kurz, W. A. 2008. Derivation of a spatially-explicit 86-year retrospective carbon budget for a landscape undergoing conversion from old-growth to managed forests on Vancouver Island, BC. *For. Ecol. Manage.* **256**, 1677–1691.

Waring, R. H. and Running, S. W. 1998. *Forest Ecosystems: Analysis at Multiple Scales* 2nd Edition. Academic Press. London UK.

Zha, T., Barr, A. G., Black, T. A., McCaughey, J. H., Bhatti, J. and co-authors. 2009. Carbon sequestration in boreal jack pine stands following harvesting. *Global Change Biol.* **15**, 1475–1487.